NASA TECHNICAL NOTE

NASA TN D-2052

THE DESIGN OF SAILPLANES FOR OPTIMUM THERMAL SOARING PERFORMANCE

by Clarence D. Cone, Jr.

Langley Research Center
Langley Station, Hampton, Va.

NATIONAL AERONAUTICS AND SPACE ADMINISTRATION • WASHINGTON, D. C. • JANUARY 1964

TECHNICAL NOTE D-2052

THE DESIGN OF SAILPLANES FOR OPTIMUM THERMAL SOARING PERFORMANCE

By Clarence D. Cone, Jr.

Langley Research Center
Langley Station, Hampton, Va.

NATIONAL AERONAUTICS AND SPACE ADMINISTRATION

For sale by the Office of Technical Services, Department of Commerce,
Washington, D.C. 20230 -- Price $1.25

THE DESIGN OF SAILPLANES FOR OPTIMUM THERMAL SOARING PERFORMANCE[1]

By Clarence D. Cone, Jr.

SUMMARY

The meteorological aspects of isolated buoyant convections (thermals) are discussed in relation to efficient soaring plane design, and the fundamental performance equation for soaring in such convections is derived. A design procedure for determining the optimum solution of the performance equation under specified thermal conditions is presented. The procedure integrates the simultaneous effects of meteorological, aerodynamic, and structural factors on soaring performance. The design procedure is illustrated in the calculation and analysis of the design charts for a conventional-geometry sailplane intended for efficient thermal soaring. Various aspects of designing for adequate gliding qualities are also discussed.

INTRODUCTION

In the development of any aircraft the mission requirements ultimately dictate the design. In the particular case of sailplanes, development of a design is complicated by the fact that efficient overall performance requires that the craft satisfy the demands of two separate missions, those of the energy-extraction or soaring phase and those of the energy-utilization or gliding phase. In the soaring phase, the sailplane must be able to extract the energy of the invisible and somewhat unpredictable vertical air currents and to store this energy in the potential form as altitude. In the gliding phase, the craft must be able to make efficient use of this energy in performing some specified task, such as goal or distance flight. Unfortunately, the aerodynamic demands of each phase are such that the design for optimum soaring is, in most cases of practical interest, quite different from that necessary for efficient gliding flight. This basic difference requires a compromise of the final design.

In the past, this compromise has usually favored maximum efficiency in gliding performance. The result has been an aircraft possessing desirable gliding qualities, but with such limited soaring dependability that practical

[1]The information contained in this publication was originally prepared for and presented at the 1961 Technical Symposium of the Soaring Society of America, Los Angeles, California, September 16, 1961 in a paper entitled "The Design and Performance Optimization of the Thermal Sailplane." By arrangement with the Society, the present expanded version is being released by NASA to increase availability.

operation is feasible only when extensive and powerful energy sources are available. The reason for the direction of this compromise is that most modern sailplanes have been built primarily for high performance in gliding competitions where emphasis is placed upon distance and speed capabilities. Under appropriate conditions and when flown by highly experienced pilots, admirable performances in these events can indeed be attained with such specialized gliders, but this performance is generally limited to the few days each year when sufficiently favorable weather conditions exist. The frequency of occurrence of such conditions in most areas is too small to permit practical soaring with such craft.

For practical soaring, what is needed is a sailplane that can perform certain and sustained flight with daily regularity, under all but dangerously stormy weather conditions. With such a craft, local goal and goal-and-return flight could be reduced to a daily routine. With such a craft, the primary practical limitations to soaring, namely, its relative uncertainty and geographical restrictions, could be removed. To attain such performance, a sailplane must obviously be designed for high efficiency in the extraction of atmospheric energy. More specifically, the craft must be able to utilize the most widely distributed energy source of the atmosphere, the free thermal. (See refs. 1 and 2.) The aircraft which fulfills these requirements, therefore, may aptly be called the "thermal sailplane." To design the craft which will meet these goals, an intimate knowledge of thermal phenomena is mandatory. Since thermal conditions vary widely from area to area and from season to season, the design of a given thermal soaring plane must fully reflect the meteorological conditions of its own specific operational area if the maximum soaring potential is to be realized.

The basic problem in the design of a thermal sailplane is the determination of the optimum balance among the various meteorological, aerodynamic, and structural factors involved in order to obtain the most efficient machine. In addition, there are the secondary problems of providing good stability, control, and maneuverability. The objective of this paper is to discuss quantitatively the more important aspects of these basic problems of thermal sailplane design and to provide a general procedure by which an optimum design can be established for a given body of thermal data and a given aircraft construction technique.

SYMBOLS

A	aspect ratio
a	vortex-ring core radius
b	wing span
C_D	total aircraft drag coefficient
$C_{D,i}$	induced drag coefficient
$C_{D,p}$	parasite drag coefficient

$C_{D,\infty}$	wing profile drag coefficient
C_L	lift coefficient
C_l	rolling-moment coefficient
c	wing chord
c_d	section drag coefficient
c_l	section lift coefficient
E	modulus of elasticity
g	gravitational constant
H	altitude
k	span efficiency factor
L/D	lift-drag ratio
L'	lift loading intensity
l	rolling moment
q	dynamic pressure
R	vortex-ring radius
r	radial coordinate; radius of turn
S	wing area
S_π	equivalent parasite drag area
V	flight velocity
V'	ascending speed of a thermal shell
V_c	circling velocity in a turn
V_w	headwind speed
V_x	horizontal gliding speed in still air
V_x'	ground speed in a glide
v	relative vertical velocity in a thermal

v_r	relative radial velocity in a thermal
u	absolute vertical velocity of air in a thermal
W	gross weight
y	spanwise coordinate
$\dot{z}$	aerodynamic sinking velocity
α	angle of attack
β	angle of sideslip
Γ	vortex-ring circulation
Γ_0	circulation in center plane of wing
γ	structural weight coefficient
δ	optimization factor
η	vertical coordinate in a thermal shell
θ	glide angle
ρ	air density
σ	thermal formation frequency
φ	angle of bank
ψ	radius of turn factor

Subscripts:

min	minimum value
max	maximum value
o	condition at outside wing tip
i	condition at inside wing tip
b	ballast

Superscript:

*	optimum value

METEOROLOGICAL BASIS OF THERMAL SOARING

The most universally distributed and potentially valuable source of soaring energy appears to be the free thermal. (See refs. 1 and 2.) A lack of knowledge of the true nature of the velocity fields of such convections has, in the past, retarded the development of an efficient thermal soaring plane. Recent advances in meteorological knowledge, however, particularly the development of the quantitative theory of the thermal shell and discovery of the mechanism of equilibrium thermal flight, have provided foundations upon which the design and construction of efficient thermal sailplanes can now proceed.

Structure and Motion of Free Thermals

The general theory of the free thermal has been treated in reference 2 and is discussed here only briefly. In principle, the free thermal closely approximates a buoyant vortex ring system in which the ring-to-core-radius ratio R/a is a relatively small number ($R/a \leqq 10$). As the buoyant ring rises, it is accompanied by an enclosing body or shell of cooler air which it has gathered from its surroundings, as shown in figure 1(a). This cooler air continuously circulates in closed streamlines around the vortex core and passes upward through the ring with high velocity and downward on the outside of the ring with a much lower velocity. The entire motion is symmetrical with respect to the vertical axis of the shell (η-axis of fig. 1(b)). This circulatory motion results in a continuous upward current over the center region of the shell; the free thermal is thus a self-sustained localized vertical current which maintains its power by the work of its buoyancy and, being completely free of any connection with the ground, floats along with the horizontal wind as it rises.

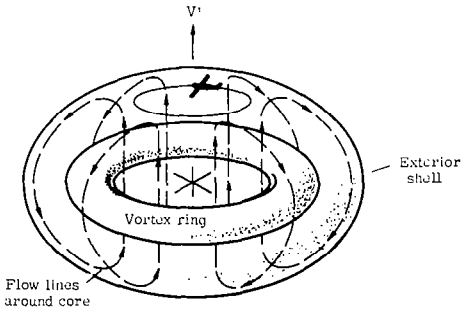

(a) Internal structure.

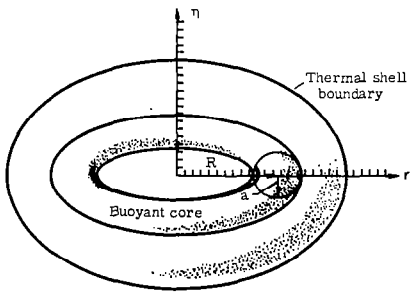

(b) Axis system.

Figure 1.- Internal flow structure of a thermal shell.

Since the velocity field of a vortex ring can be determined mathematically, the velocity field within a given thermal shell can be calculated when certain physical properties and dimensions of the equivalent vortex ring are known. The velocity V' with which the thermal shell rises is given by

$$V' = \frac{\Gamma}{4\pi R}\left(\log_e \frac{8R}{a} - \frac{1}{4}\right) \qquad (1)$$

and when the effective values for the circulation Γ, the ring radius R, and the core radius a are given, the entire velocity field can be specified. The buoyancy of the vortex core causes the thermal shell to enlarge and to alter its velocity field slowly as it rises.

When the effective values of Γ, R, and a are specified for a particular thermal shell, a plot of the vertical component v of the velocity field within the shell can be made; this plot is called a thermal diagram. Such a plot is shown in figure 2 for a thermal with $R/a \approx 5$. The diagram is nondimensional and applies to any size thermal for which $R/a \approx 5$. This diagram shows the distribution of the vertical velocity relative to the core as a function of radial distance r for various η-planes parallel to the core plane and was obtained from experimental data for the measured velocity field of a small buoyant convection shell in a water tank. (See ref. 2.) The dimensional thermal diagram (v plotted against r; η, constant) can be obtained from figure 2 by multiplying the vertical and horizontal scales by the values of V' and R, respectively, for any particular thermal with $R/a \approx 5$. The absolute vertical velocity of the air at any point in the thermal relative to earth is given by

$$u = V'\left(\frac{v}{V'} + 1\right) \tag{2}$$

where V' is calculated from equation (1).

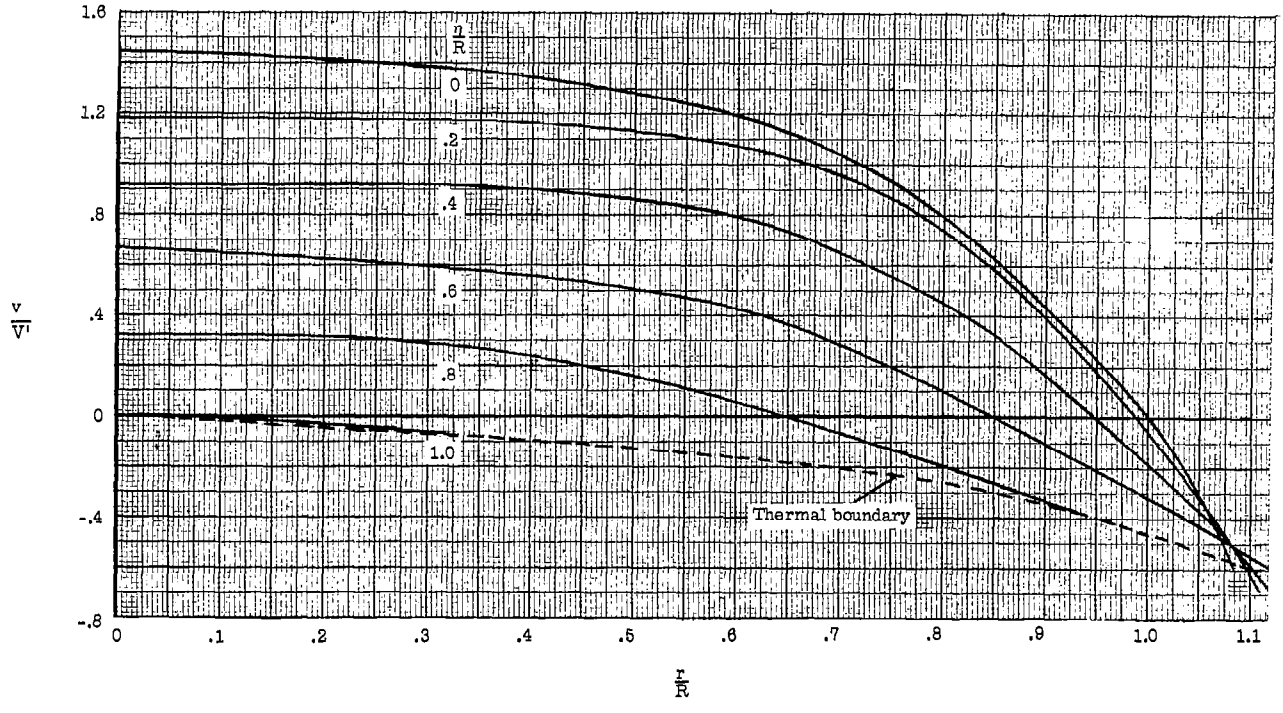

Figure 2.- Thermal diagram for vertical velocity field. $\left(\text{Nondimensional, } \frac{R}{a} \approx 5\right)$.

In general, the vertical components of the air motion within the thermal shell are of primary interest, since it is these currents which govern the availability of the thermal energy for soaring. However, because of the circular motion of the air around the vortex core, lateral or radial velocity components also exist, and although these components are usually small and of little importance in large thermals where the sailplane can circle in the almost pure central upcurrent, they may have a pronounced effect on the stability of sailplanes operating in thermals which are small compared with the wing span of the craft. A nondimensional plot of the relative radial velocity v_r in the top half of a thermal with $R/a \approx 5$ is presented in figure 3. For the bottom half of the shell the pattern would be approximately the same, only the flow would be inward toward the η-axis. This figure shows that the radial velocities become large only near the boundary of the thermal shell and directly above the vortex core.

Flight Within Thermal Shells

If a sailplane enters the top half of a thermal shell and begins circling with a radius r about the vertical η-axis, it will initially rise or sink relative to the core until some η-level is reached where the value of v is equal to the aerodynamic sinking velocity $\dot{z}$ at that radius. At such a level, the thermal

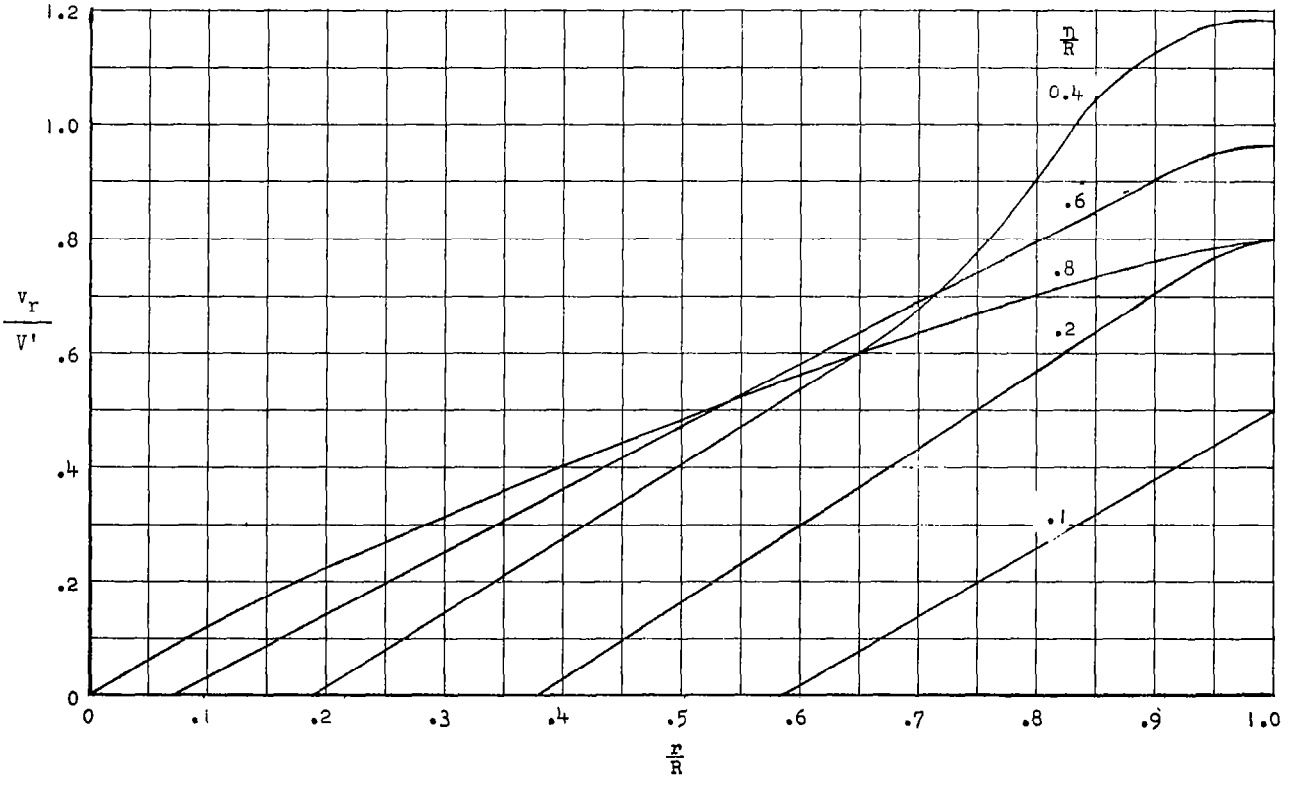

Figure 3.- Lateral velocity field of a thermal shell. $\left(\text{Nondimensional, } \frac{R}{a} \approx 5\right)$.

will "capture" the sailplane and carry it along. If such a level can be found, the craft will attain a state of stable equilibrium with respect to the core and can maintain this position within the shell; ultimately, it will be carried to the maximum useful altitude reached by the thermal. Attainment of equilibrium, of course, requires that the thermal be large enough and intense enough to satisfy the aerodynamic characteristics and power requirements of the particular sailplane. If the thermal is too small or too weak for equilibrium flight, that is, $\dot{z} > v$ everywhere in the thermal, the sailplane will sink relative to the core and must ultimately pass out of the shell. However, while thus sinking (relative to the core), the craft may actually have gained altitude if $(V' + v) > \dot{z}$. The difference in available energy, depending on whether equilibrium is reached, can be very large. It is therefore obvious that the fundamental requirement for maximum efficiency in the use of a given thermal by a given sailplane is that equilibrium flight be possible for at least one radius of turn.

An important factor in the ability of a sailplane to reach equilibrium involves the capability of the craft to make turns of sufficiently small radius. (See fig. 2.) For example, suppose that a certain sailplane can fly in the thermal represented by figure 2 at a minimum value of $r/R = 1.0$ with a minimum sinking velocity $\dot{z}$ such that $\dot{z}/V' = 0.1$. Then, as is obvious from the diagram, equilibrium cannot be attained anywhere in the thermal. If, however, the sailplane could perform a turn of radius such that $r/R = 0.3$, the sinking velocity of the craft could increase to 14 times its initial value and the plane would still be able to attain equilibrium and make maximum use of the thermal. This condition illustrates an important fact in thermal soaring: a relatively inefficient aircraft can still perform thermal soaring with maximum altitude gain, provided it can execute turns of sufficiently small radius. The case here is that a quite adequate power supply exists if only the craft can get deep enough into the thermal to use it.

If a sailplane enters a thermal below the core plane (η negative), equilibrium flight would still be possible, but the motion would be unstable since v increases continuously toward the core plane ($\eta = 0$). This condition is illustrated in figure 4 which shows the variation of v/V' with vertical distance η/R in the thermal. The magnitude and sign of the derivative $\frac{\partial(v/V')}{\partial(\eta/R)}$ measures the magnitude and nature of the level stability of a given circling orbit r,η. When the slope of the curves is positive (that is, in the region where $\eta/R < 0$), the equilibrium is unstable. Thus, a slight deviation from the equilibrium position would send the craft either climbing to the upper half of the thermal or else sinking completely out of the shell. It is therefore unlikely that any appreciable amount of equilibrium circling flight can be accomplished in the lower half of the thermal shell.

In addition to this instability of the orbit level, the air motion in the region of the bottom stagnation point of the shell will not correspond exactly to the ideal vortex ring flow. Because of the buoyancy of the core, the impulse of the system must increase as the shell rises in unstable or neutrally stable air and the size of the shell will usually increase, especially during the early stages of formation. The additional air added to the shell is taken in at the very bottom so that in this region the shell is not actually closed as in the

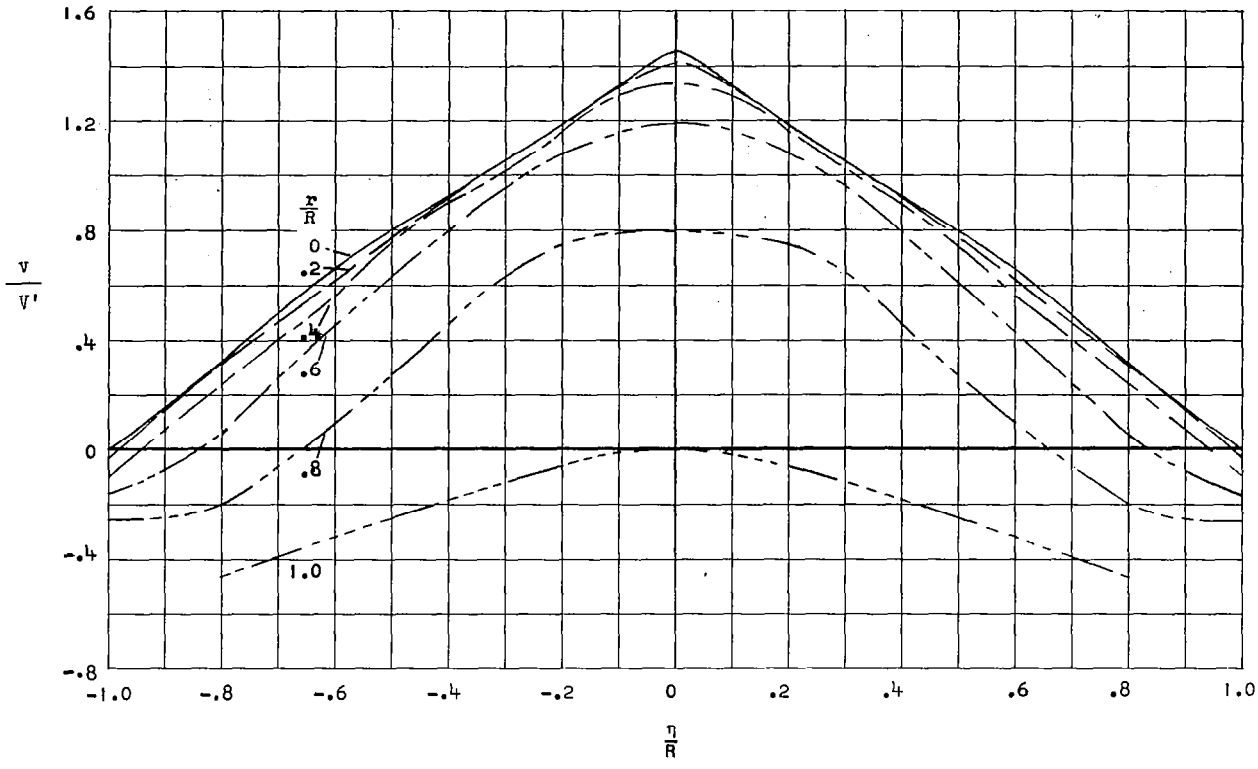

Figure 4.- Equilibrium stability diagram. $\left(\text{Nondimensional, } \frac{R}{a} \approx 5\right)$.

ideal system. A sailplane flying below a rapidly growing shell might therefore be quickly sucked up into the top half of the thermal by this bottom upflow. There are also vertical currents flowing upward (relative to earth) for some distance above and below the shell due to the so-called "drift flow" associated with the vertical motion of the thermal mass through the air. (See ref. 3.)

Certain additional considerations of stability of circling flight and thermal distributions are presented in appendixes A and B, respectively.

FUNDAMENTAL PERFORMANCE EQUATION OF THERMAL SOARING

Maximum utilization of thermal energy requires that equilibrium with the thermal be established. Equilibrium in a given thermal requires not only that the craft be able to circle within the upcurrent region but also that within some part of this region the aerodynamic sinking velocity be equal to the vertical velocity of the air relative to the thermal core. Thus, the relation between $\dot{z}$ and r is of critical importance since it determines the minimum thermal size and strength that can be used. The function $\dot{z}(r)$ constitutes the fundamental performance equation of thermal soaring flight.

Derivation of Performance Equation

The rather complex absolute motion of a sailplane in a thermal can be resolved into two simpler components, the motion of the craft relative to the air and the motion of the air relative to the earth. The latter component can be determined by use of the thermal theory; it is set by atmospheric conditions, being the given energy source which nature provides, and is quite beyond our power to alter or control. The former component, however, is fully open to alteration, subject only to the limitations of engineering and construction abilities. Shaping the sailplane's motion pattern to fit that of the air motion is thus the basic problem of thermal soaring design and is analogous to the balancing of power available by power required in internal powered aircraft design. The motion of the craft relative to the air is completely expressed by $\dot{z}(r)$.

A consideration of the force and velocity equilibriums in a spiral glide (ref. 2) results in the following parametric equations for $\dot{z}(r)$:

$$\dot{z} = \left(\frac{W}{S}\right)^{1/2}\left(\frac{2}{\rho}\right)^{1/2} \frac{C_D}{\left[C_D^2 + \left(C_L \cos \varphi\right)^2\right]^{0.75}} \tag{3}$$

$$r = \left(\frac{W}{S}\right)\left(\frac{2}{\rho g}\right)\frac{C_L \cos \varphi \cot \varphi}{C_D^2 + \left(C_L \cos \varphi\right)^2} \tag{4}$$

where φ is the angle of bank in the turn. These equations can be validly simplified by noting that, for sailplanes, $C_D^2 \ll C_L^2 \cos^2\beta$, and therefore the effects of C_D^2 can be neglected. The fundamental performance equation, in parametric form, becomes

$$\dot{z} = \left(\frac{W}{S}\right)^{1/2}\left(\frac{2}{\rho}\right)^{1/2} \sec^{1.5}\varphi \, \frac{C_D}{C_L^{1.5}} \tag{5}$$

$$r = \left(\frac{W}{S}\right)\left(\frac{2}{\rho g}\right)\frac{\csc \varphi}{C_L} \tag{6}$$

By using any desired function for $\varphi(r)$, the performance equation $\dot{z}(r)$ can be plotted by varying C_L, an experimental or theoretical drag polar being used to determine C_D as a function of C_L. With $\dot{z}(r)$ thus established, it is possible to determine the thermal performance of the craft. It should be noted, as mentioned in reference 2, that a drag polar which accounts for the effects of circling flight on the drag should be used with equations (5) and (6) if these effects are sufficient to cause appreciable deviation from the straight flight polar.

Method of Performance Analysis

Superposition of the $\dot{z}(r)$ curve on the dimensional thermal diagram of any given thermal will immediately show whether equilibrium can be attained and will also show the exact regions of the thermal within which the craft can fly in equilibrium. In particular, when used with the "design" thermal, $\dot{z}(r)$ will show the degree to which the design requirements can be met. This procedure is illustrated in figure 5 which shows a hypothetical thermal diagram with the $\dot{z}(r)$ equation for two different sailplanes superposed. In the case of craft A, $\dot{z}(r)$ does not intersect $v(r)$ for any η-level in the thermal and hence equilibrium cannot be established. Sailplane B, on the other hand, has an appreciable region available over which equilibrium can be attained.

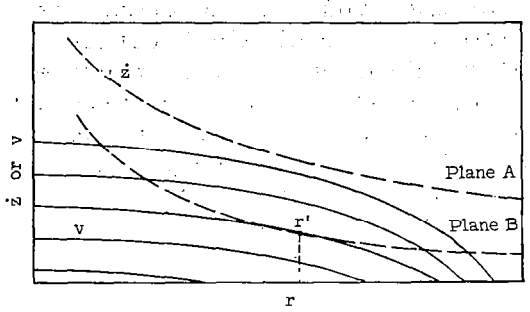

Figure 5.- Use of thermal diagram for performance analysis.

It is interesting to note that, except for the highest level, there are two values of the radius of turn for each η-level where equilibrium can exist. No matter where in the equilibrium region the craft flies, it will still rise with the same vertical velocity V' as does the entire shell. If, however, the craft is attempting to gain altitude rapidly, some initial gain in rate of climb can be obtained if the thermal is entered at a low level, by flying at radius r' as shown in figure 5. This radius corresponds to the highest equilibrium η-level in the thermal and the sailplane initially will rise rapidly to this level from a lower one.

It is obvious that for equilibrium thermal flight it is desirable that $\dot{z}(r)$ be as small as possible. For the larger thermals this condition insures a large equilibrium region and greatly reduces the need for accurate control of the circling flight path; for the smaller thermals, it is a mandatory condition if equilibrium is to be achieved. For certainty of flight, the $\dot{z}(r)$ curve must be flat enough to allow the smallest, weakest thermals to be used. The various aerodynamic and structural factors which determine $\dot{z}(r)$ will now be analyzed with a view to finding the craft design which will best satisfy this requirement.

DESIGN PROCEDURE FOR OPTIMUM SOLUTION OF PERFORMANCE EQUATION

The problem of determining the minimum value of $\dot{z}(r)$ for an existing sailplane is first considered; and then the more important case of designing an optimum craft is discussed.

Evaluation of Existing Sailplanes for Thermal Soaring

The expressions for the sinking velocity and radius of turn are given by equations (5) and (6). For the case of an existing sailplane, the various factors

which are needed to determine $\dot{z}$ and r are already available. The flight wing loading W/S is known and the relation between C_D and C_L is given by the drag polar for the particular craft. In general, this polar is the lift-drag relation for straight gliding flight, but can usually be safely used for estimating performance in turns because the minimum radius of turn is very large compared with the span for most existing sailplanes. If, however, the craft can attain a minimum radius of turn of the same order of magnitude as the span, the polar for circling flight may vary considerably from that for straight flight. This variation is due to the asymmetric lift loading introduced by the spanwise gradients of velocity, sideslip, and angle of attack, as well as to the large drag increments associated with the trim control necessary in small turns. In such cases, a polar which accounts for these effects must be used. For very small turns this polar will be a function of the radius of turn. With the use of equations (5) and (6), the sinking velocity may be calculated as a function of r for any desired variation of φ.

The optimum combination of lift coefficient and bank angle.- In general, a sailplane can make a turn of given radius by use of any number of suitable combinations of lift coefficient and bank angle. However, since $\dot{z}$ is affected by both C_D and φ, one particular combination of C_L and φ might be expected to produce a minimum sinking velocity. The remaining problem therefore is the determination of the optimum combination of C_L and φ so that $\dot{z}$ will be a minimum at each radius of turn. To determine this relation, equation (6) is rewritten in the form,

$$C_L \sin \varphi = \left(\frac{W}{S}\right)\left(\frac{2}{\rho g}\right)\frac{1}{r} = \psi \tag{7}$$

where ψ is obviously a constant for a given radius of turn, that is, the product $C_L \sin \varphi$ determines the radius. Since W/S and ρ are constants, choice of a series of values for r will give a corresponding series of values for ψ. Now $\dot{z}$ can be expressed as a function of ψ by the following substitutions:

$$\dot{z} = \left(\frac{W}{S}\frac{2}{\rho}\right)^{1/2} \frac{C_D}{(C_L \cos \varphi)^{1.5}} = \frac{C_D}{\left(\sqrt{C_L^2 \cos^2 \varphi}\right)^{1.5}} (gr\psi)^{1/2} \tag{8}$$

or

$$\dot{z} = \frac{C_D}{\left(\sqrt{C_L^2 - \psi^2}\right)^{1.5}} (gr\psi)^{1/2} \tag{9}$$

For a constant value of ψ (corresponding to a specific radius of turn) $\dot{z}$ will be a minimum when the parameter

$$\frac{\left(\sqrt{C_L^2 - \psi^2}\right)^{1.5}}{C_D} = \delta \tag{10}$$

is a maximum. Therefore, if a plot is made of C_L against δ for a constant value of ψ, the value of C_L for which δ is a maximum gives the optimum lift coefficient C_L^* for that radius and this C_L value then determines the optimum angle of bank φ^*, according to the relation

$$\varphi^* = \sin^{-1}\left(\frac{\psi}{C_L^*}\right) = \sin^{-1}\left(\frac{W}{S}\frac{2}{\rho g}\frac{1}{rC_L^*}\right) \tag{11}$$

Plots of C_L^* or the corresponding α^*, and φ^* against radius of turn will give the optimum combination of angle of attack and bank for minimum sinking speed in circling flight.

The minimum sinking velocity in turns.- The corresponding minimum value of the sinking velocity for each radius becomes

$$\dot{z}_{min} = \frac{C_D^*}{\left(\sqrt{C_L^* - \psi^2}\right)^{1.5}}(gr\psi)^{1/2} \tag{12}$$

where C_L^* is the optimum lift coefficient for the particular radius of turn and C_D^* is the corresponding drag coefficient. With this information, the minimum sinking velocity curve $\dot{z}_{min}(r)$ can be constructed; when this curve is superposed on the thermal diagram, the performance of the craft can be directly evaluated.

Optimum-Design Procedure for a Thermal Soaring Plane

The more important problem of the total design of a sailplane for maximum efficiency in thermal soaring will now be considered. To evolve a truly optimum design, it would be necessary to have a detailed knowledge of the thermal distributions for the geographical area or areas over which the craft is to soar. The craft would then be designed for use of a sufficiently small minimum thermal size, the "design" thermal, such that the total frequency of usable thermals would assure certainty of sustained flight.

The drag polar.- The basic design problem consists of determining the optimum balance among the various structural and aerodynamic parameters appearing in the fundamental performance equation (eqs. (5) and (6)) so that $\dot{z}(r)$ has its minimum possible value and r_{min} is also very small. Before proceeding with the design considerations, it is convenient to expand the drag polar of equation (5)

into its components so that the individual effects of the various drag sources may be more clearly seen. Thus,

$$C_D = C_{D,p} + C_{D,\infty} + \frac{C_L^2}{\pi kA} \tag{13}$$

Here $C_{D,p}$ is the parasite drag coefficient and is obtained from the equivalent flat-plate drag area S_π by dividing by the wing area S; (that is, $C_{D,p} = S_\pi/S$). The wing profile drag coefficient for the selected wing section $C_{D,\infty}$ usually varies rather strongly with C_L, and $C_L^2/\pi kA$ is the induced drag coefficient where A is the geometrical aspect ratio and k is the efficiency factor that accounts for the deviation of the lift loading from the optimum elliptical form. In general, for small turns, k is a function of the radius. By using this drag polar form in equation (5), the performance equations can then be written as

$$\dot{z} = \left(\frac{W}{S}\right)^{1/2}\left(\frac{2}{\rho}\right)^{1/2}\left(\sec^{1.5}\varphi\right)C_L^{1.5}\left(C_{D,p} + C_{D,\infty} + \frac{C_L^2}{\pi kA}\right) \tag{14}$$

$$r = \left(\frac{W}{S}\right)\left(\frac{2}{\rho g}\right)(\csc\varphi)C_L^{-1} \tag{15}$$

A rather complex interaction exists between the aerodynamic and structural parameters in both of these equations. For instance, if the span of the design is set, and A is allowed to increase, W/S also increases. A larger value of A means a lower value of $\dot{z}$, aerodynamically, especially for the high C_L values necessary in small radius turns. The accompanying increase in W/S, however, increases $\dot{z}$ as well as the radius of turn and thus tends to cancel the benefits of the larger aspect ratio. Additionally, increasing A necessarily increases the thickness ratio of the wing sections; thus, with normal wing sections, $C_{D,\infty}$ increases and also tends to negate the benefits of the increase in A. Ultimately, the increase in $C_{D,\infty}$ with increase in A completely overcomes the reduction in $C_{D,i}$, even at moderate lift coefficients. Also, if the wing loading and maximum lift coefficient are such that the wing span is an appreciable percentage of the minimum radius of turn, the factor k (eq. (13)) can become a significant function of r for small turns since the wing loadings are no longer elliptical. Under such conditions $C_{D,p}$ may also become a function of r; this condition will be discussed later. These interactions occurring in circling flight can pose considerably more involved design problems than is the case for straight gliding flight.

The span length.- The first step in the present design procedure is to determine the span length. The selection of an optimum span for the thermal soarer is not a simple matter, but two fundamental conditions aid in the choice. The first is the requirement of low W/S. Small spans generally mean lower gross

weights for a given wing area. This weight reduction is in the form of lower wing structural weight because of the smaller wing spars and lower fuselage and empennage weights. The second condition involves the adverse effects encountered by large-span wings in turns of small radius. The nature of these effects is discussed in appendix A. The thermal soarer must have a low wing loading for efficient circling flight and therefore would be able to attain sufficiently small circles wherein these effects are important.

Various criteria can be set up for this purpose. For example, a "design" minimum circling radius, as determined from thermal data, can be set. The maximum allowable span can then be calculated on the basis of the requirement that when executing a turn of this design radius, the 90-percent semispan, or some other tip section of the inner wing, will still be some specified percentage below the stall angle of attack for the section, with a realistic value for φ. Another, but more involved, criterion for use in selecting the span would be a detailed analysis of the actual rolling moments and trim requirements of given spans at the design radius, by using a probable wing loading or of the total drag increases associated with the design radius of turn.

The wing loading.- With the wing span chosen, the various factors and coefficients occurring in equations (14) and (15) must be determined so that the performance equation can be calculated. It is convenient to express these as functions of the aspect ratio. The factors involved in the determination of the wing loading are considered first. Since

$$S = \frac{b^2}{A} \tag{16}$$

the aspect ratio sets the wing area; it also determines the structural wing loading. To determine the wing loading as a function of the wing geometry and construction technique to be used, the gross flight weight W of the craft can be expanded into its component parts as follows:

$$W = W_o + W_S + W_b + W_f \tag{17}$$

where

W_o weight of pilot plus auxiliary equipment

W_S structural weight of wing due to area

W_b structural weight of wing due to span (primarily spar weight)

W_f structural weight of fuselage and empennage

These structural weight components can in turn be expressed in terms of weight functions:

$$\left.\begin{aligned} W_S &= \gamma_S S \\ W_b &= \gamma_b b^3 \\ W_f &= \gamma_f b \end{aligned}\right\} \tag{18}$$

where the γ coefficients are empirically determined or theoretically estimated constants which depend in value on the materials and techniques of construction. The specific expressions used here for the weight functions are arbitrary, but in general the form depends somewhat on the construction technique and materials used. More involved relations can be used, of course, such as those given by Wilkinson (ref. 4). However, care must be taken that the sailplanes used in the statistical derivation of such empirical relations are actually constructed with materials and techniques similar to those to be employed on the actual aircraft under design. Derivations based on large numbers of dissimilar sailplanes are not sufficiently accurate for specific design work. For new techniques and materials, specific weight functions must, of course, be developed by theoretical or experimental procedures. The functions used here have proven quite representative for conventional sailplanes of wooden construction having very low wing loadings. Since a low wing loading is very necessary for thermal soaring in order to circle at the "design" radius, these relations show the need for using structural materials and methods which will make the γ values sufficiently small and still meet the strength requirements. By using equations (16) and (17), the gross flight wing loading expressed as a function of wing span and aspect ratio becomes

$$\frac{W}{S} = W_o \frac{A}{b^2} + \gamma_S + \gamma_b bA + \gamma_f \frac{A}{b} \tag{19}$$

The wing profile drag.- The next factor of importance to be determined is the function $C_{D,\infty}$. The selection of an optimum wing section in order to minimize $C_{D,\infty}$ at the higher lift coefficients where the craft will operate is also dependent on the aspect ratio. As has already been mentioned, a large aspect ratio requires a thick profile, and thickness ratio has a pronounced effect on both the $C_{D,\infty}$ and $C_{L,max}$ of wing sections. For the NACA 4- and 5-digit airfoil series, $C_{L,max}$ decreases beyond a thickness ratio of about 12 percent, whereas the minimum value of $C_{D,\infty}$ increases steadily with thickness increase. It is clear, therefore, that for these normal sections the aspect ratio must be held to a low enough value to allow sections of moderate thickness to be used. In general, it would be quite advantageous to use the very low drag laminar-flow sections characterized by the NACA 6-series airfoils. Unfortunately, nearly all of these profiles, although very efficient in the lift-coefficient range of the drag "bucket," generally have very high drag values for C_L above this range, even higher than those of the 4- and 5-digit series. It is, of course, the region of high lift coefficients which is of primary interest in thermal soaring.

There are, however, some laminar airfoils which have the valuable property that increasing thickness causes the low drag bucket to shift to the higher C_L

region with only a small increase in the minimum drag. Such sections, for example, the NACA 653-618, appear to hold much promise for application to thermal soaring planes. This particular section has a $C_{D,\infty}$ value of only 0.0061 at $C_L = 1.0$, with a $C_{L,max}$ of 1.3 at a Reynolds number of 3×10^6. The maximum L/D of this section occurs at $C_L = 1.04$. Although the minimum drag value increases slightly as the Reynolds number decreases, the range of C_L values over which the low drag exists increases. It thus appears that some exceptionally favorable profiles are available for specific use in design of the thermal soarer.

The parasite drag.- The remaining factor to be determined in equation (14) is the parasite drag coefficient $C_{D,p}$ which includes trim drag and is usually considered to be independent of angle of attack or lift coefficient. The parasite drag coefficient $C_{D,p}$ plays an important role in determining the sinking velocity of a sailplane and should always be reduced to its lowest possible value. The parasite drag coefficient can be reduced by eliminating as much fuselage and empennage area as possible and by paying strict attention to such drag-producing details as fuselage-wing junctures, canopy contour and fairing, control gaps, miscellaneous protuberances, and prevention of all areas of separated flow. Generally, the parasite drag coefficient can be expressed in terms of an equivalent flat-plate drag area S_π obtained by summing the equivalent areas of all the parasite-drag producing components; $C_{D,p}$ is then obtained by the relation

$$C_{D,p} = \frac{S_\pi}{S} \tag{20}$$

Generally, S_π will have a value which is nearly independent of wing area, and $C_{D,p}$ will decrease as the aspect ratio decreases

$$C_{D,p} = \frac{S_\pi}{b^2} A \tag{21}$$

Optimization procedure.- With the value of b determined, choice of a value for the aspect ratio will determine the wing area, the wing loading, and the parasite drag coefficient by use of equations (16), (19), and (21), respectively. Since $C_{D,\infty}$ is also known for the selected profile, all the factors necessary for determining the circling performance curve $\dot{z}(r)$ from equations (14) and (15) are available. There remains only the need for optimizing the performance curve. This is done in exactly the same manner as outlined in the preceding section for the case of an existing design by use of the $\psi - \delta$ procedure. Since the drag polar of the design aircraft is now available, the optimization procedure reduces to that for a craft with known characteristics.

For the selected span length, a series of optimum performance curves $\dot{z}_{min}(r)$ can be determined for any desired range of values for the aspect ratio. A plot of these curves will then indicate very clearly the optimum value or range of values for the aspect ratio, when used in conjunction with the design turn radius or the model thermal diagram. In this way, the effects of aspect ratio on

all the various aerodynamic and structural parameters can be integrated, and the optimum value selected for any specified construction technique. In addition, the optimization calculations also yield the optimum values C_L^*, or α^*, and φ^* for minimum sinking speed at each radius.

It is assumed in the foregoing procedure that the best available or best possible values for the various parameters will be used, consistent with the materials and methods to be used for construction. The performance charts will then indicate whether these parameter values will allow the craft to attain the desired design performance. On the other hand, by suitably varying the individual parameters and calculating the associated performance curves, the necessary values which the various parameters must have in order to attain a given performance can be ascertained. Whether such values can actually be realized in a sailplane will depend entirely upon the physical limitations of the construction methods available. In any case, the design procedure can be used to establish the optimum performance possible with a given technique or to specify the values which must be attained to meet a given performance requirement.

CALCULATION AND ANALYSIS OF PERFORMANCE CHARTS

In order to illustrate the use of the foregoing procedure and to provide information useful for the preliminary design of thermal soaring planes, a set of performance curves has been prepared for a design series which is assumed to adhere closely to the general geometry layout of conventional sailplanes and which also assumes that conventional construction techniques are utilized. The charts are considered to be representative of sailplanes which can be realized with current state-of-the-art practices. The particular values used for the structural weight coefficients and the equivalent flat-plate drag area are representative of rather efficient design and construction methods and the charts, although realistic, are not intended to be conservative. These charts are analyzed in this section and in the following section to illustrate their use in obtaining the optimum design for both the soaring and gliding phases of flight.

Performance Chart Calculation

Performance charts have been calculated for three different span lengths: 30, 40, and 50 feet. For each of these spans, the optimum performance curve $\dot{z}_{min}(r)$ was calculated for each of five aspect ratios: 5, 8, 10, 15, 20. This aspect ratio range covers all practical cases. For calculation purposes, the basic (not optimum) performance equation can be expanded in terms of the structural constants and drag coefficients to yield

$$\dot{z} = \left(W_o \frac{A}{b^2} + \gamma_S + \gamma_b bA + \gamma_f \frac{A}{b}\right)^{1/2} \left(\frac{2}{\rho}\right)^{1/2} \left(\sec^{1.5}\varphi\right) C_L^{-1.5} \left(S_\pi \frac{A}{b^2} + C_{D,\infty} + \frac{C_L^2}{\pi k A}\right) \qquad (22)$$

$$r = \left(W_o \frac{A}{b^2} + \gamma_S + \gamma_b bA + \gamma_f \frac{A}{b}\left(\frac{2}{\rho g}\right)(\csc \Phi) C_L^{-1}\right) \tag{23}$$

These equations can be easily programed for solution by machine computation for any desired input of constants and functions. The particular values of the constants and functions used in the computation of the illustrative performance curves are:

W_o = 190 lb (weight of pilot and equipment)

γ_S = 0.73 lb/sq ft

γ_f = 2.1 lb/ft

γ_b = 0.000125 lb/cu ft

g = 32.2 ft/sec^2

ρ = 0.002378 slug/cu ft

S_π = 1.0 sq ft

k = 1.0

$C_{D,\infty}$ = drag polar for the NACA 64_3-618 airfoil section

The weight constants used are characteristic of wooden construction and are empirically determined from data for early sailplanes which generally had much lighter structures than present-day craft do. By using these coefficient values, the wing loading can be expressed as

$$\frac{W}{S} = 190 \frac{A}{b^2} + 0.73 + 2.1 \frac{A}{b} + \left(1.25 \times 10^{-4}\right) bA \tag{24}$$

This relation has been plotted in figure 6 for the three span lengths. Two important facts are obvious from this plot. First, the wing loading increases linearly with the aspect ratio at a rate which depends upon the span length. Secondly, the larger the span, the lower the wing loading for a given aspect ratio. The reason for the smaller value of W/S for larger spans with the same A is, of course, that the increase in wing area lowers the wing loading due to the basic weight more than the wing loading increases because of the span increase. Thus, a low wing loading appears to require a large span and a small aspect ratio.

In order to illustrate the validity of equation (24) in predicting the wing loading, the value of W/S as calculated by this equation has been entered in figure 6 as a solid symbol for several actual sailplanes. The measured wing loading of the actual craft is entered as an open symbol. It is obvious that equation (24) very adequately predicts the wing loadings, especially since the

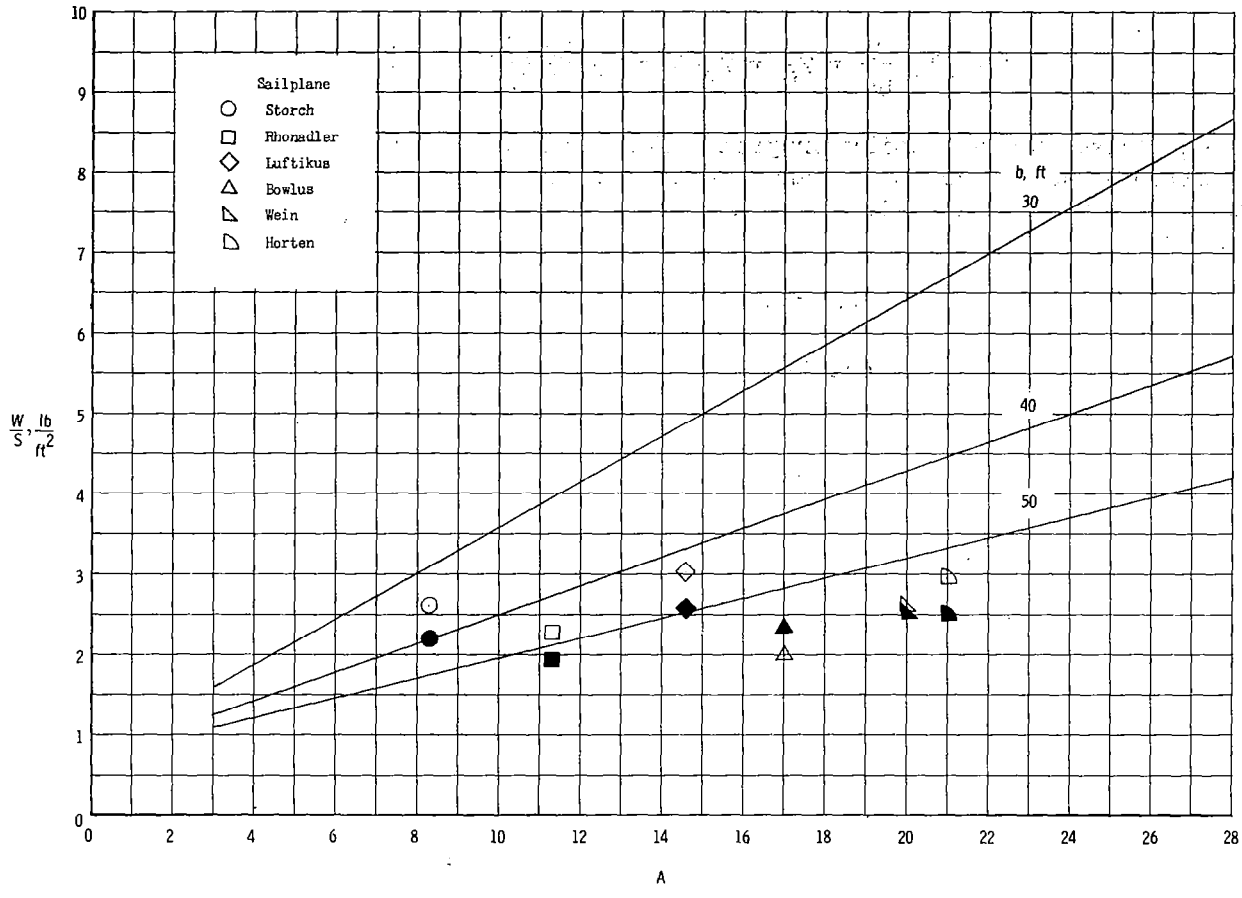

Figure 6.- Variation of wing loading with aspect ratio for constant span lengths. The value W/S calculated by equation (24) for specific sailplane is indicated by a solid symbol.

weight functions used are purposely intended to be indicative of considerably more efficient construction than that of the actual sailplanes used for the comparison.

The wing efficiency factor of 1.0 is reasonably valid for the smaller spans if the wing is designed for elliptical loading. A value $k = 1.0$ is considered very optimistic for the 50-foot span in small turns. This value for k assumes, of course, that careful attention has been paid to canopy and fuselage-wing juncture design. The choice of a value of S_π of 1.0 square foot is very realistic for the two smaller spans, but is very optimistic for the largest span in tight turns because of trim drag.

The optimum choice of wing section is somewhat dependent upon the secondary flight phase, especially with use of a laminar-flow section. More will be said concerning this subject in the next section. The choice of the NACA 64_3-618 was based on the very low drag of the profile at high lift coefficients and on the extensive range of the low drag bucket $\left(0.2 \leqq C_L \leqq 1.1\right)$, which makes this airfoil

ideal for the overall flight range. The aerodynamic characteristics of this section as measured in the NASA low-turbulence wind tunnel at a Reynolds number of 3×10^6 are presented in figure 7. The characteristics of other suitable profiles are presented in references 5 and 6.

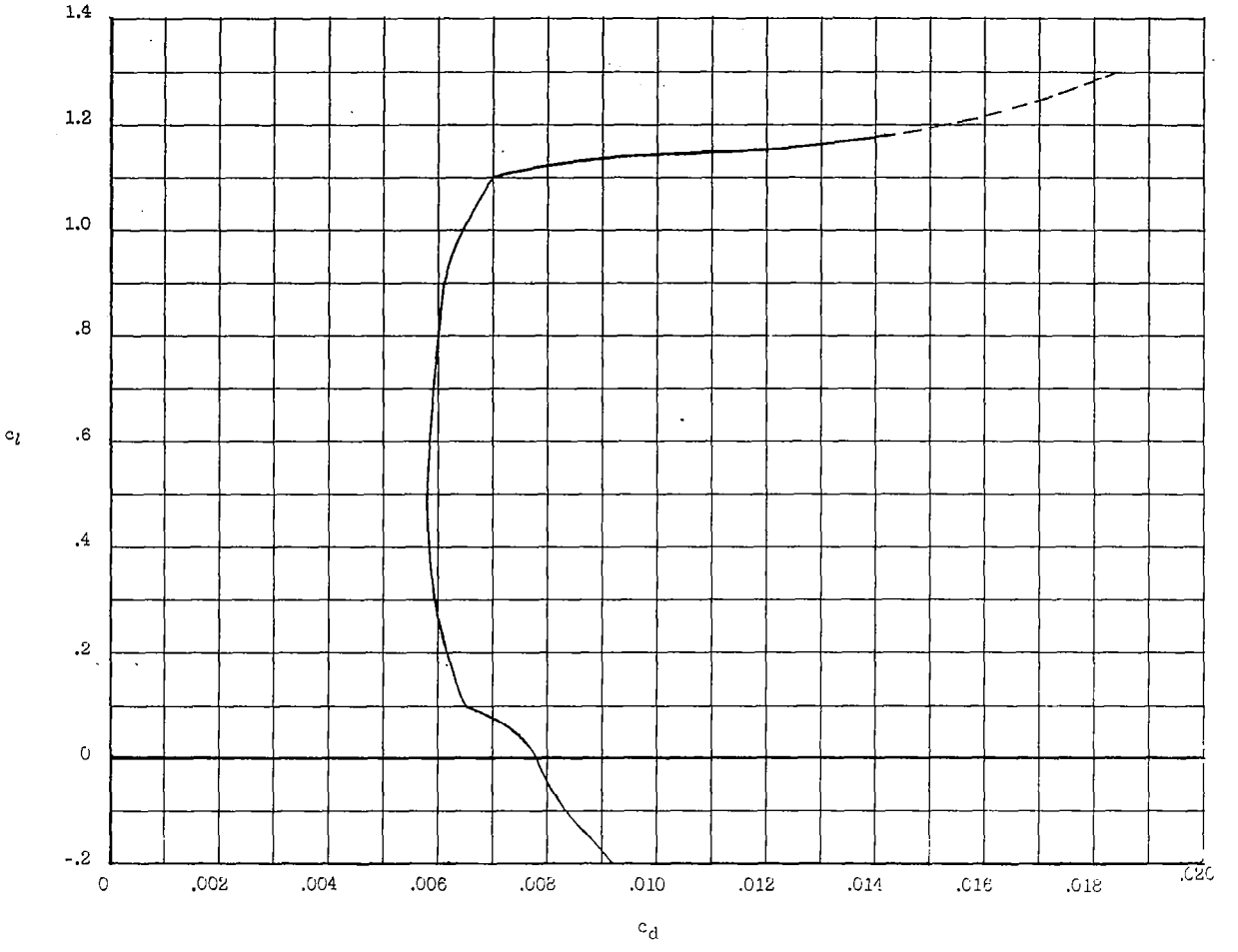

Figure 7.- Profile drag polar for the NACA 643-618 section.

Analysis of the Performance Charts

The calculation of $\dot{z}_{min}(r)$ was carried out for each span and aspect ratio according to the foregoing optimization procedure. A sample plot of the relation C_L plotted against δ for constant ψ values is presented in figure 8 for the case of $b = 40$ feet, $A = 15$. The final performance charts are presented in figure 9. A comparison of these figures indicates a distinct performance advantage by using the largest span ($b = 50$ feet). This apparent advantage stems from the lower wing loading which occurs with the larger spans for a given aspect ratio. In reality, the performance curves of figure 9(c) are not truly valid for the smaller radii of turn because of the adverse effects occurring with large

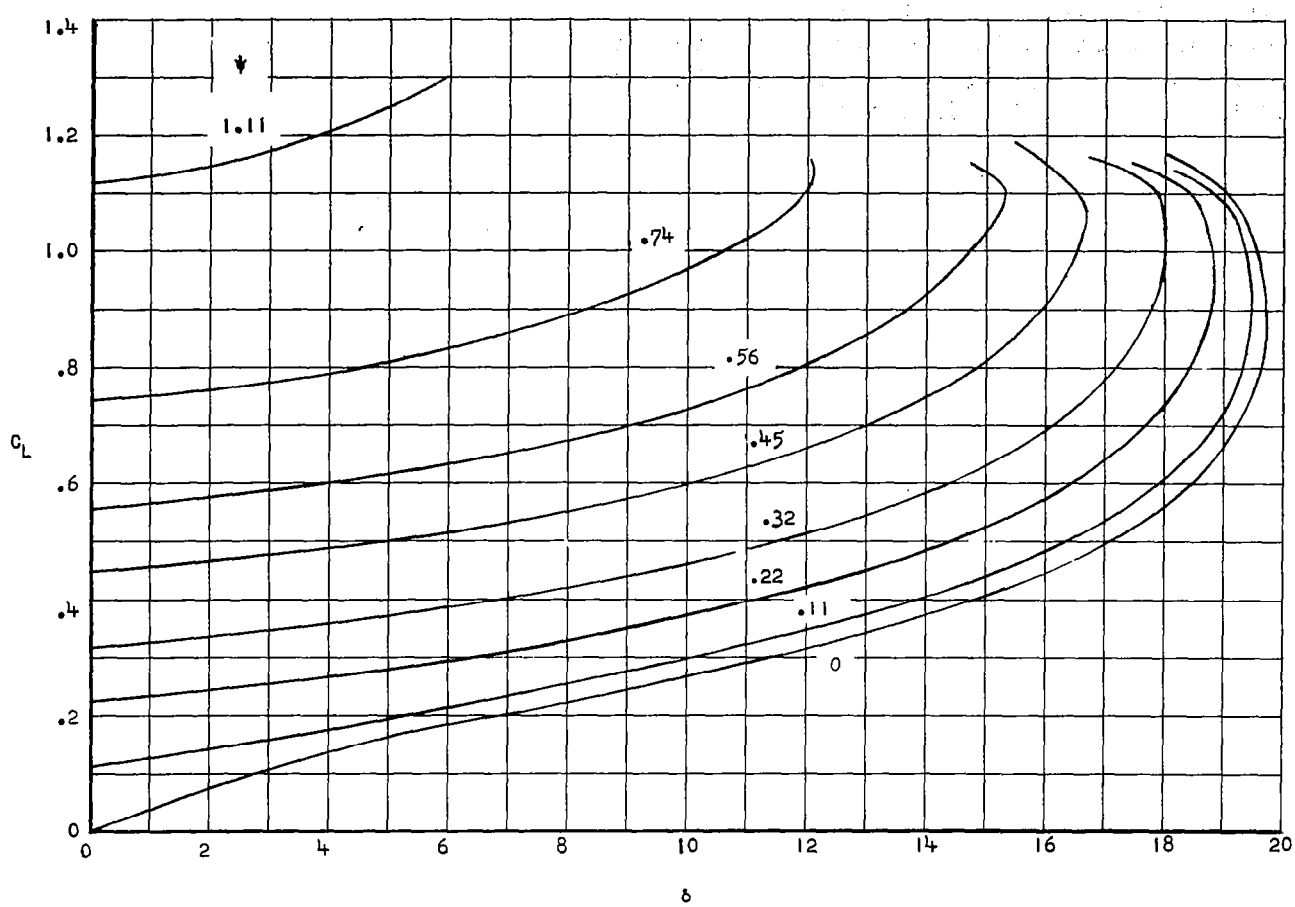

Figure 8.- Variation of δ with C_L for constant ψ values. b = 40 feet; A = 15.

spans, as discussed in appendix A. The increase in total drag due to these effects would very probably raise the sinking velocity considerably for r-values below about 125 feet. For the larger values of r, the curves of figure 9(c) are valid and clearly illustrate the advantage of low wing loading in obtaining a flat $\dot{z}_{min}(r)$ curve. For the 40-foot span (fig. 9(b)) the sinking velocity in small turns can be kept to reasonable values by use of the smaller aspect ratios. The high wing loading occurring with the 30-foot span (fig. 9(a)) makes the sinking velocity large for even medium size turns.

For purposes of analysis, further discussion is limited to the case of designs with spans of 40 feet. (See fig. 9(b).) The curves of figure 9(b) clearly indicate the necessity of using relatively small aspect ratios for low sinking velocities in small turns. In general, the smaller the turn, the lower the aspect ratio must be for efficient flight. The curves also indicate that in no case does a large aspect ratio ($A \geqq 20$) produce the minimum sinking velocity, not even in straight gliding flight ($r = \infty$). It appears that the minimum $\dot{z}$ in gliding flight occurs for $A \approx 15$. The minimum radius of turn is shown in

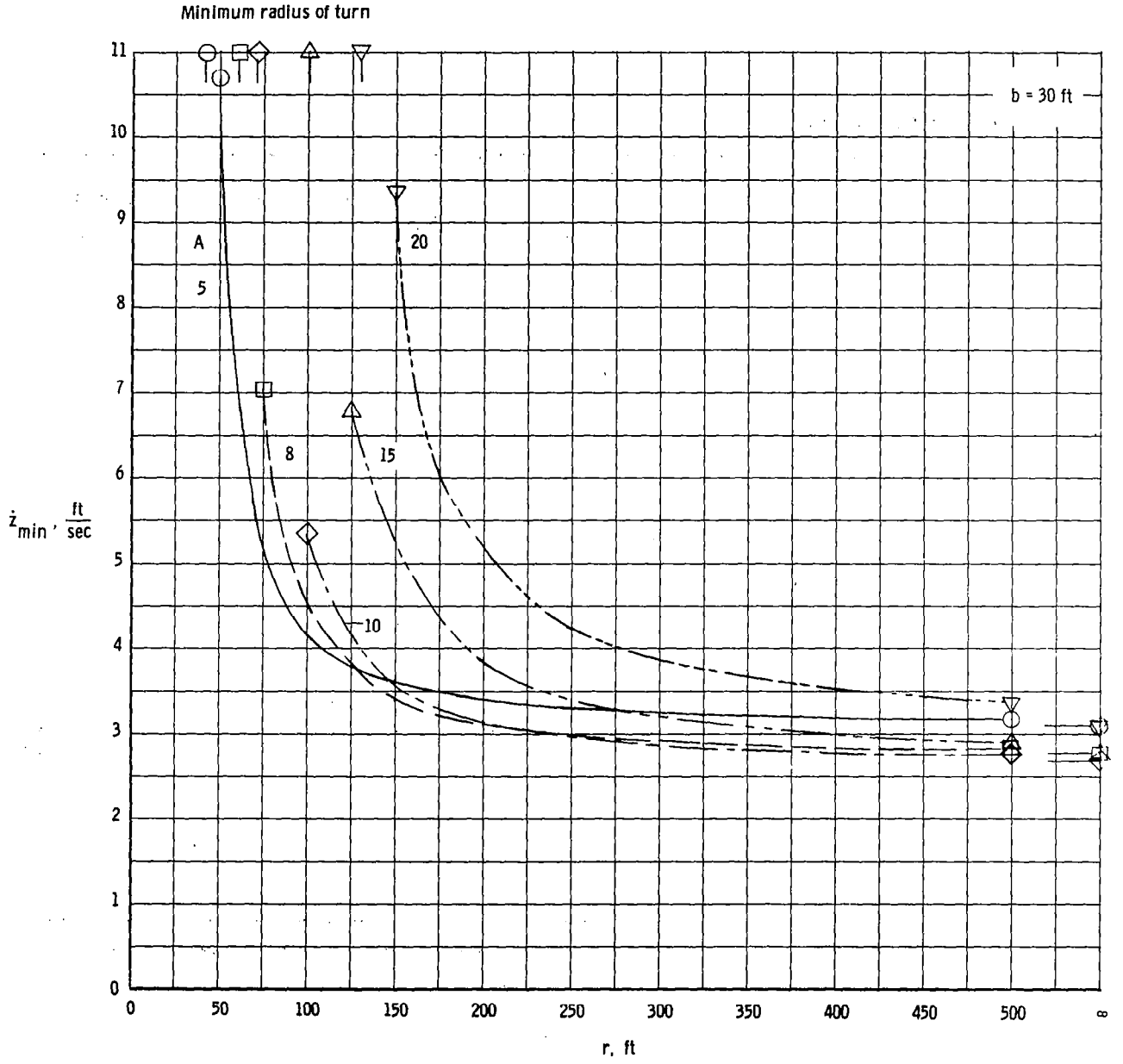

(a) b = 30 feet.

Figure 9.- Performance curves for various aspect ratios.

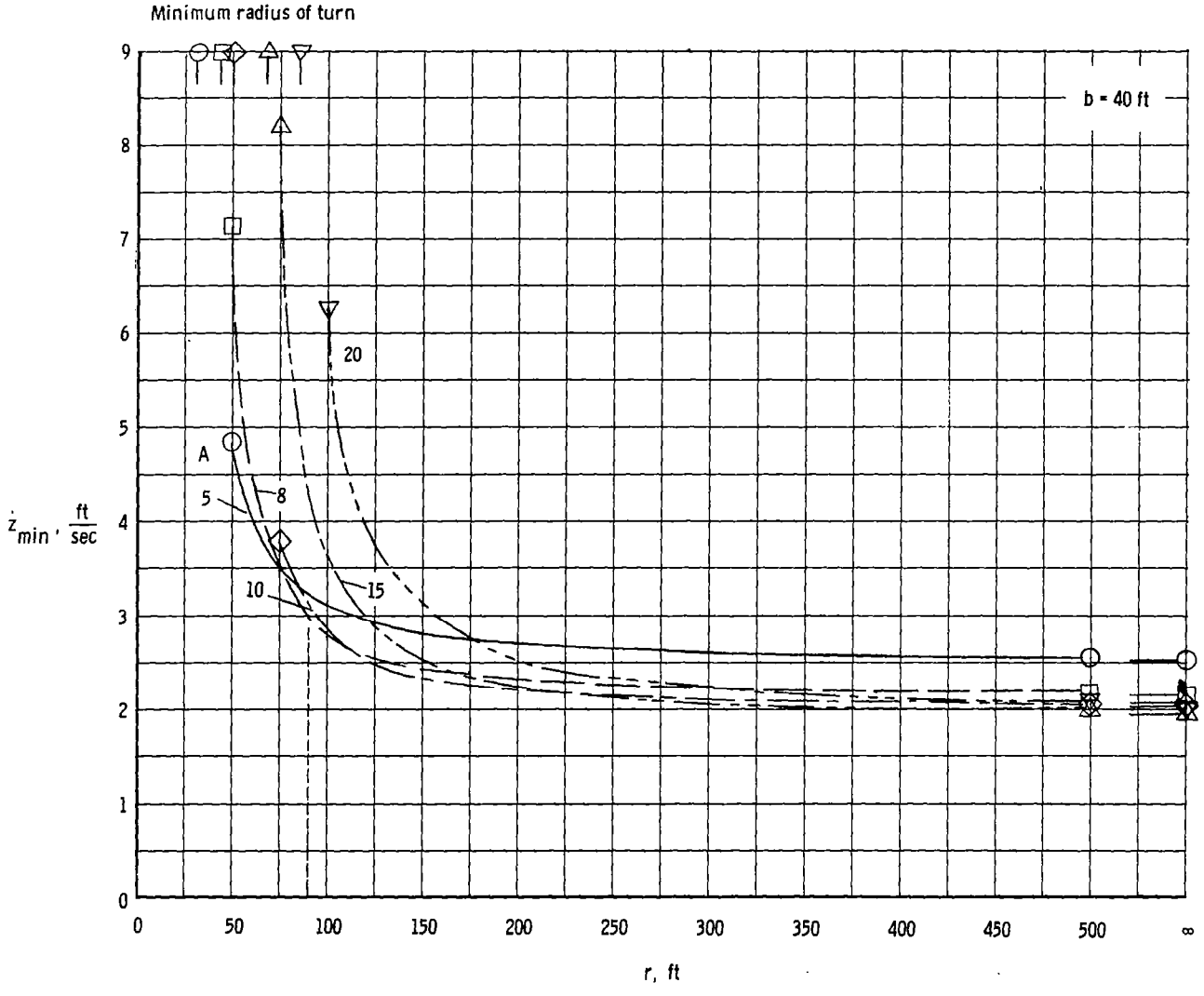

(b) b = 40 feet.

Figure 9.- Continued.

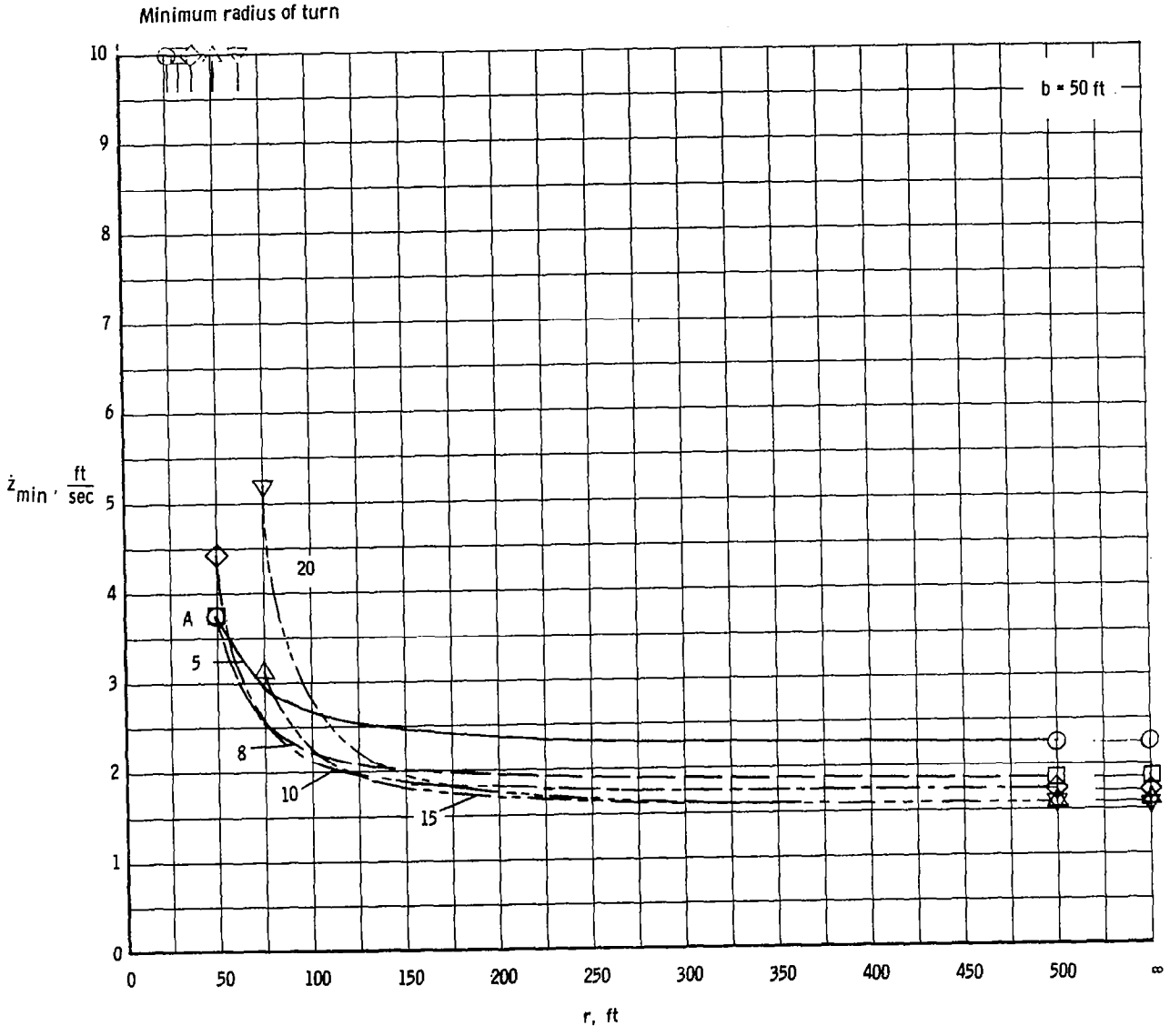

(c) b = 50 feet.

Figure 9.- Concluded.

figure 9(b) and it is seen that r_{min} also decreases with decreasing aspect ratio, because of the decreasing wing loading. These curves show that with a 40-foot span a sailplane could circle at a radius of 90 feet with a minimum sinking velocity of 3 feet per second for values of A between 8 and 10. From available thermal data, this low sinking velocity appears to be adequate for the attainment of equilibrium within thermals.

The optimum aspect ratio, therefore, appears to lie in the region $8 \leqq A \leqq 10$, an aspect ratio near 10 being more desirable for larger radii. For very small turns, aspect ratios less than 8 are more efficient, but b/r and $\dot{z}$ then become so large that this region of aspect ratios is of little practical interest. It is obvious that great improvements in circling efficiency are still possible at all aspect ratios if only the total wing loading could be reduced while the 40-foot span is maintained.

Optimum Flight Angles

To illustrate the variation of the optimum lift coefficient C_L^* and the optimum bank angle φ^* with radius of turn, figure 10 has been prepared for the specific case of the $b = 40$ feet, $A = 8$ design for which the performance curve is given in figure 9(b). It is seen that both C_L^* and φ^* increase slowly as r decreases and that even for small turns ($r = 90$ feet), φ^* is still relatively small ($\varphi^* = 33.5^\circ$). For the particular design constants chosen, the interactions are such that the craft must be flown at a high lift coefficient $\left(C_L^* \geqq 0.9\right)$ for minimum sinking velocity, even for turns of large radius. If it is assumed that the downwash is constant across the span and that the load distribution experienced in small turns is essentially the same as in straight flight, C_L^* may be used to determine the optimum angle of attack α^*. The trend of the variation of C_L^* and φ^* with r is the same for the other aspect ratios of figure 9(b).

Summary of Circling Flight Design

To summarize the results of the performance calculations of this section, it appears that a sailplane with a span of 40 feet and an aspect ratio of 8 to 10, and possessing the stated design characteristics, would be capable of performing equilibrium flight within small thermals the relative velocity of which in the core plane at a radius of 90 feet is at least 3 feet per second. Such a craft can be constructed with presently available techniques. However, improved circling performance is still possible if the wing loading of the craft could be reduced. Because of the low wing loading of this particular design ($W/S = 2.14$ pounds per square foot), only moderate optimum angles of bank are required in small turns.

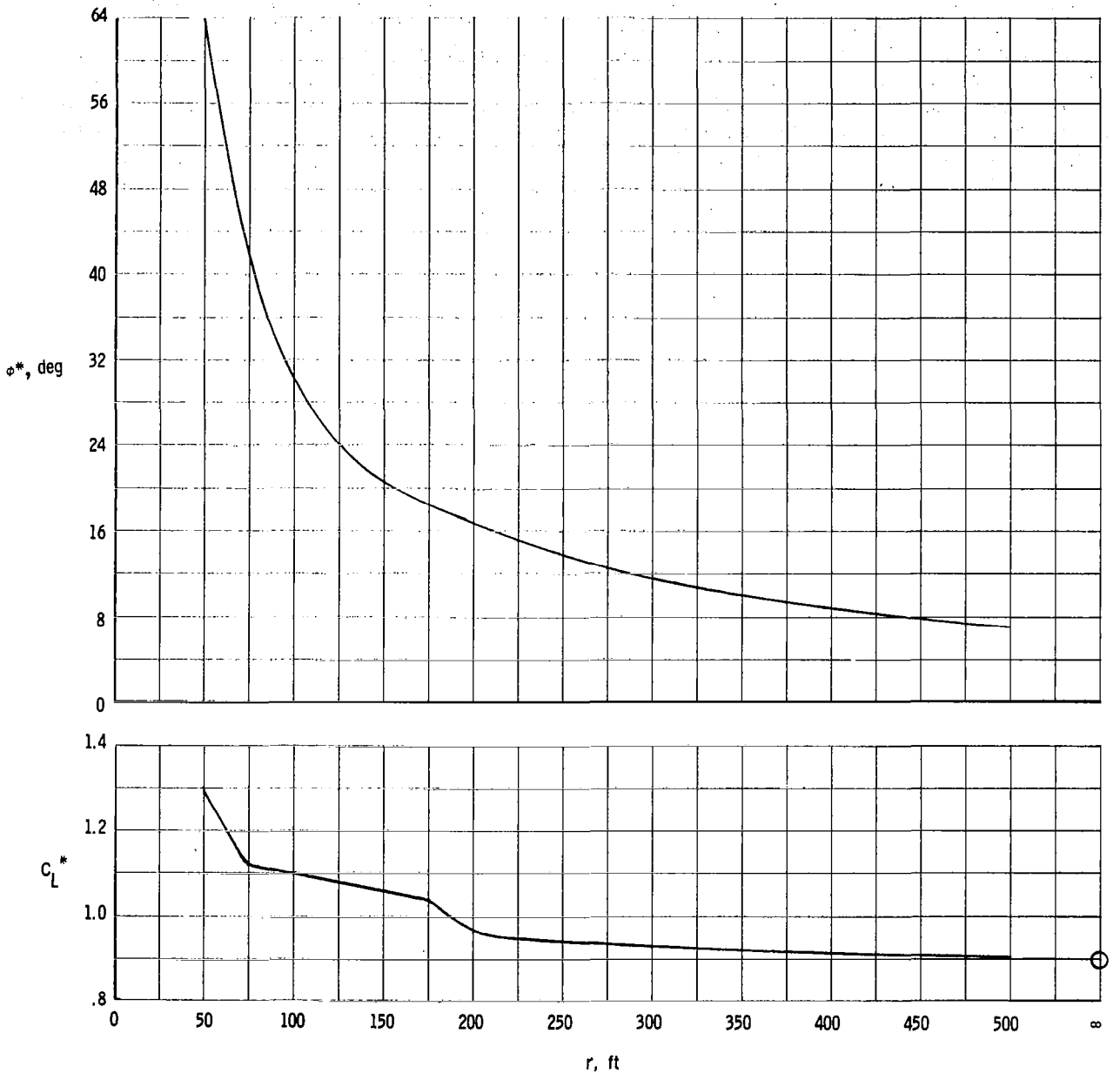

Figure 10.- Variation of optimum lift coefficient and bank angle with radius of turn. b = 40 feet; A = 8.

DESIGN FOR THE COMPLETE FLIGHT RANGE

In general, it is desirable to do more than just make continuous circles within thermals and for truly practical soaring it is necessary that the craft also be able to use its potential energy of altitude for reasonably efficient straight gliding flight to a preset goal or to return to its home field. More specifically, the craft must possess the necessary penetration power to reach a preset destination under normal or average headwind conditions. If it is assumed then that by use of the foregoing procedure a preliminary design has been selected on the basis of optimum soaring ability, it is now necessary to examine the gliding flight characteristics to see what compromise of the design, if any, must be made to obtain the desired gliding efficiency.

Gliding Requirements

In order to have reasonable gliding performance, two requirements must be met: the gliding angle θ must be reasonably small and the wing loading must be large enough to give sufficient ground speed in moderate headwinds. Satisfaction of the second requirement guarantees that a thermal soaring plane will be able to perform preset goal and return flights with a high degree of reliability. The requirement of low wing loading for efficient thermal flight and high wing loading for penetration are, of course, incompatible so that some compromise may be necessary just as in the case of the high-performance sailplane. For the thermal soarer, this compromise need not be so severe, however, since only moderate ground speeds are required and since the craft design will be tailored to the meteorological conditions of its own particular geographical area.

Gliding Angle

A small gliding angle requires a large value of L/D as indicated by the relation

$$\theta = \cot^{-1} \frac{L}{D} \tag{25}$$

The smaller this angle, the greater will be the efficiency of the craft in using its potential energy of altitude for covering ground distance in still air. The lift-drag ratio is given by

$$\frac{L}{D} = \frac{C_L}{\frac{S_\pi A}{b^2} + C_{D,\infty} + \frac{C_L^2}{\pi k A}} \tag{26}$$

and the expression for θ becomes

$$\theta = \cot^{-1} \frac{C_L}{\frac{S_\pi A}{b^2} + C_{D,\infty} + \frac{C_L^2}{\pi k A}} \qquad (27)$$

When this relation is plotted as a function of C_L for the optimum thermal design, the gliding angle may be read directly, and the minimum value of θ determined by inspection. If $C_{D,\infty}$ can be expressed analytically, θ_{min} can be solved for by the usual minimization process. This value will, of course, indicate only the calm-air gliding efficiency of the craft, whereas for the actual ground-speed efficiency, the headwind must also be considered.

The problem of adjusting the design, if necessary, to obtain a given value of $(L/D)_{max}$, or θ_{min}, reduces to an analysis of the effects of the various factors in equation (27). In general, increases in $(L/D)_{max}$ can best be obtained by a reduction of the values of S_π and $C_{D,\infty}$, since this procedure also reduces the value of $\dot{z}_{min}$ in turns. However, if $(L/D)_{max}$ is increased by increasing the aspect ratio, the resulting design must be reevaluated from the soaring performance standpoint since the accompanying increase in wing loading will modify $\dot{z}_{min}(r)$. The procedure will then reduce to a series of trials which can be conveniently handled by graphical methods; from these trials, the most optimum compromise can be selected.

In the selection of a wing profile, it is important to choose a section which will have a low drag value over a large C_L range, since $C_{D,\infty}$ is very important in determining both circling and gliding performance with equations (22) and (27), respectively. The thick laminar-flow profiles, such as characterized by the NACA 64_3-618, appear to be especially suitable for the overall flight range since the low drag bucket extends over almost the entire practical lift range.

In order to illustrate the magnitude and variation of L/D and θ for sailplanes designed primarily for thermal soaring, figure 11 has been prepared for the same design series for which the circling performance curves are presented in figure 9(b) for $b = 40$ feet. Two interesting facts are revealed by these curves. First, the maximum value of L/D is very high even for the lowest aspect ratio ($A = 5$), and secondly, the lift coefficient at which this maximum occurs decreases as the aspect ratio decreases. The high value of $(L/D)_{max}$ means that even with the small aspect ratios required for optimum soaring (for example, $A = 8$ to 10), reasonably high gliding angles can still be attained $\left((L/D)_{max} = 24 \text{ to } 25.5\right)$. This condition in turn means that a thermal soarer with the previously described characteristics will be able to accomplish distance glides with "still-air" efficiency almost comparable to that of many of the so-called "high performance" sailplanes. It is interesting to note that the L/D curves of figure 11 have a very gradual bending near the maximum so that a large C_L range may be flown without an appreciable increase in the gliding angle. The

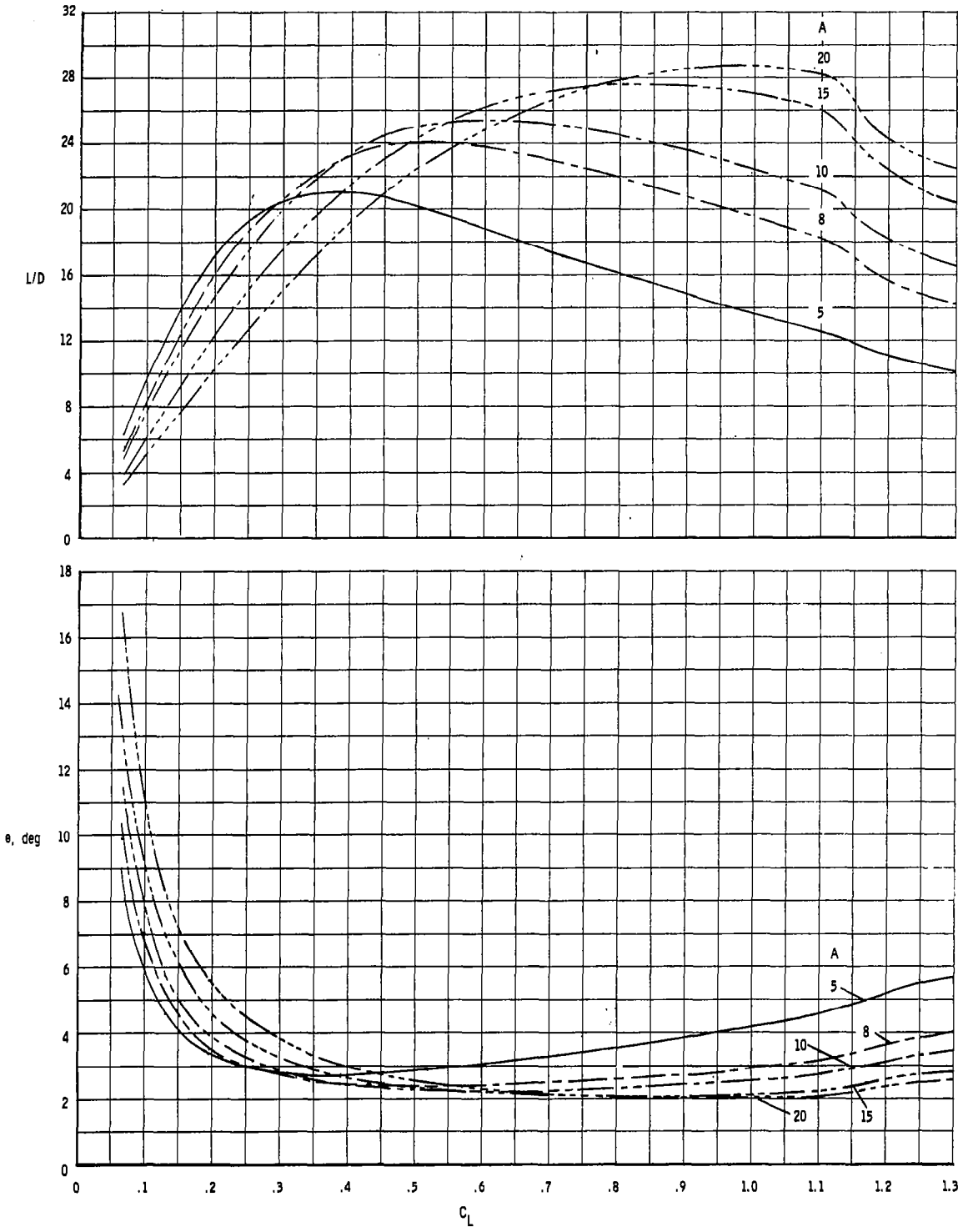

Figure 11.- Variation of L/D and θ for design with b = 40 feet and A = 8.

second point of interest, the low C_L value for $(L/D)_{max}$ which occurs with low aspect ratios, is beneficial from the standpoint of attaining adequate ground speed.

Ground Speed

The requirement of attaining sufficient ground speed depends primarily upon the wing loading. In general, a thermal soaring craft would be flown at or near the lift coefficient for $(L/D)_{max}$ so that only the wing loading affects the airspeed V, since

$$V = \left(\frac{W}{S}\right)^{1/2}\left(\frac{2}{\rho}\frac{\cos\theta}{C_L}\right)^{1/2} \tag{28}$$

Since the thermal soaring plane is not primarily concerned with extremely long distance flights, time is not of great importance and the craft will generally make the most efficient use of altitude by flying with θ near the minimum value while using a wing loading high enough to attain the necessary ground speed.

If the wing loading of the basic design is assumed to be very low, a considerable degree of control can be exercised over the airspeed by using ballast to vary the gross flying weight W and hence the gross wing loading. This procedure has long been used on high-performance gliders and is a particularly suitable means for varying the characteristics of the fixed-wing thermal sailplane to accommodate varying meteorological conditions.

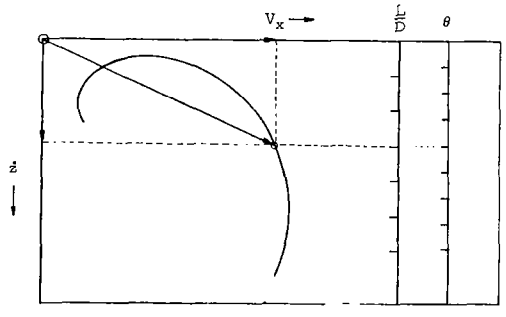

(a) General form.

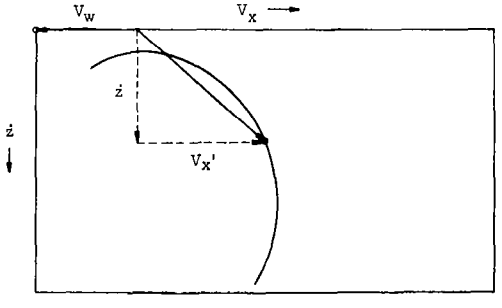

(b) Use with wind vector.

Figure 12.- Gliding diagram.

To determine the actual wing loading requirements for a given flight of a thermal soaring plane, a conventional gliding diagram, such as sketched in figure 12(a), can be constructed for the chosen design. This diagram gives the "still-air" ground speed V_x and the sinking velocity $\dot{z}$, where

$$V_x = \left(\frac{W}{S}\right)^{1/2}\left(\frac{2}{\rho C_L}\right)^{1/2}\cos^{3/2}\theta \tag{29}$$

To obtain the desired true ground speed V_x' in a given headwind V_w, the wind vector is placed on the diagram, as shown in figure 12(b), and the velocity of the craft relative to earth is read in the usual manner for any flight condition (that is, for any value of C_L). In particular, the value of

V_x' for $(L/D)_{max}$ can be read directly. The relation for determining the necessary gross wing loading W/S for a given ground speed V_x' in a headwind of V_w is simply

$$\frac{W}{S} = \frac{1}{2}\left(V_x' + V_w\right)^2 \rho C_L \cos^3\left(\cot^{-1}\frac{L}{D}\right) \tag{30}$$

For a design with a permanently fixed wing loading where ballast will not be used, a "design" headwind can be established by a statistical analysis of the wind records of a particular region and this value used to set the minimum wing loading of the craft in much the same manner as the model thermal is used to set the design for the soaring phase.

If the wing loading can be varied by setting the desired value of W before a flight, by use of ballast, the flight characteristics can be varied to suit the prevailing wind conditions. For instance, on days of low wind, the minimum value of W is desirable for maximum soaring efficiency whereas on days of very high wind an increase in W may be necessary, even at the expense of decreased soaring efficiency. Equation (30) can again be used to calculate the necessary ballast weight. This equation can be rearranged to give

$$W_b = \frac{S}{2}\left(V_x' + V_w\right)^2 \rho C_L \cos^3\left(\cot^{-1}\frac{L}{D}\right) - W_T \tag{31}$$

where W_b is the ballast weight necessary to give the desired ground speed V_x', and W_T is the basic gross weight of the craft and pilot without the ballast. When ballast is used, care must be taken that it is added very near the basic center of gravity of the craft; otherwise, the drag polar becomes a function of the ballast weight because of trim drag.

Effective Penetration Ability

Even with a relatively low wing loading, the thermal sailplane may be able to accomplish penetration of a given headwind with an overall efficiency approaching that of the more efficient, heavily loaded gliders because of the soaring ability of the lighter sailplane. Because of its ability to attain equilibrium in even small thermals and its ability to gain altitude rapidly and frequently, the thermal sailplane will need to be carried downwind a lesser distance for a given altitude gain than the slower climbing glider. Despite its lower gliding efficiency and wing loading, the soarer may still be able to cover ground distance with an average speed comparable with that of the glider. In fact, its relative certainty of finding usable thermals may allow it to continue gaining headway long after the glider has been forced to land. Actually, strong winds favor the production of many small thermals and, as has been seen, these winds are especially suited to the efficient operation of a thermal sailplane; they are, however, very useless to gliders. This state of affairs is illustrated in figure 13, where the solid curve shows the flight path of the glider and the dashed curve shows that of the soaring plane. The relative speed efficiencies

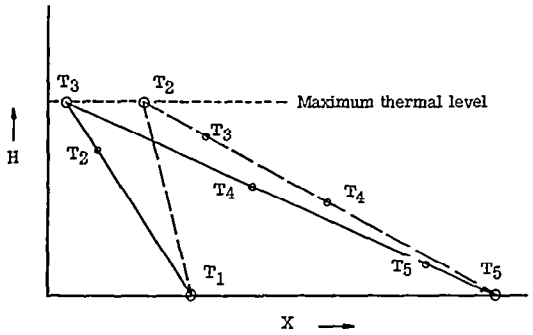

Figure 13.- Comparison of ground-speed efficiencies of a glider and a soaring plane. T denotes equal time intervals.

of the two craft will, of course, depend upon the total weather conditions, but the often marginal soaring ability of the highly loaded sailplane indicates that the thermal soarer may possess some advantages even in the aspect of wind penetration.

Illustration of Gliding Performance

To illustrate the use of the gliding diagram and to gain an idea of the ground-speed capabilities of a realistic thermal soaring plane, figure 14 has been prepared for the particular design of figure 9(b) with b = 40 feet and A = 8, which, as has already been seen, possesses optimum efficiency in small turns. This particular design attains a maximum L/D of 24 at a lift coefficient of 0.52. The corresponding values of $\dot{z}$ and V_x, respectively, are 2.4 feet per second and 58.6 feet per second or 40.1 mi/hr (1 mile = 5,280 feet). It thus appears that even in a moderately high headwind, for example, V_w = 20 miles per hour, reasonable headway can still be made with this craft. Because of the flatness of the L/D curve, the value of V_x can be increased considerably without excessive decreases in L/D. For example, V_x can be increased to approximately 51 miles per hour at $C_L = 0.33$ with an L/D of 21.5 and to 65.5 miles per hour at $C_L = 0.20$ with an L/D of 15.5. If the ability of the thermal soaring plane to work even minimum size thermals efficiently is considered, it appears that these values of V_x are sufficient for a wide range of horizontal wind velocities, even without ballast.

In the event ballast must be used, the necessary weight can be calculated by equation (31). The effect of the increased wing loading will, of course, alter the optimum circling performance curve $\dot{z}_{min}(r)$. To determine the new optimum curve after ballast addition, one needs only to use the relations:

$$\dot{z}_b = \dot{z}\left[\frac{(W/S)_b}{W/S}\right]^{1/2} \tag{32}$$

$$r_b = \frac{(W/S)_b}{W/S}\, r \tag{33}$$

where the subscript b denotes the condition with ballast, and the factors without subscripts refer to the original unballasted condition. It is important to note that in using this correction only r is modified. In effect, the original $\dot{z}_{min}(r)$ curve is merely shifted to the right by the amount $r_b - r$. The same curve shift applies to the $\varphi^*(r)$ and $C_L^*(r)$ curves; that is, after the

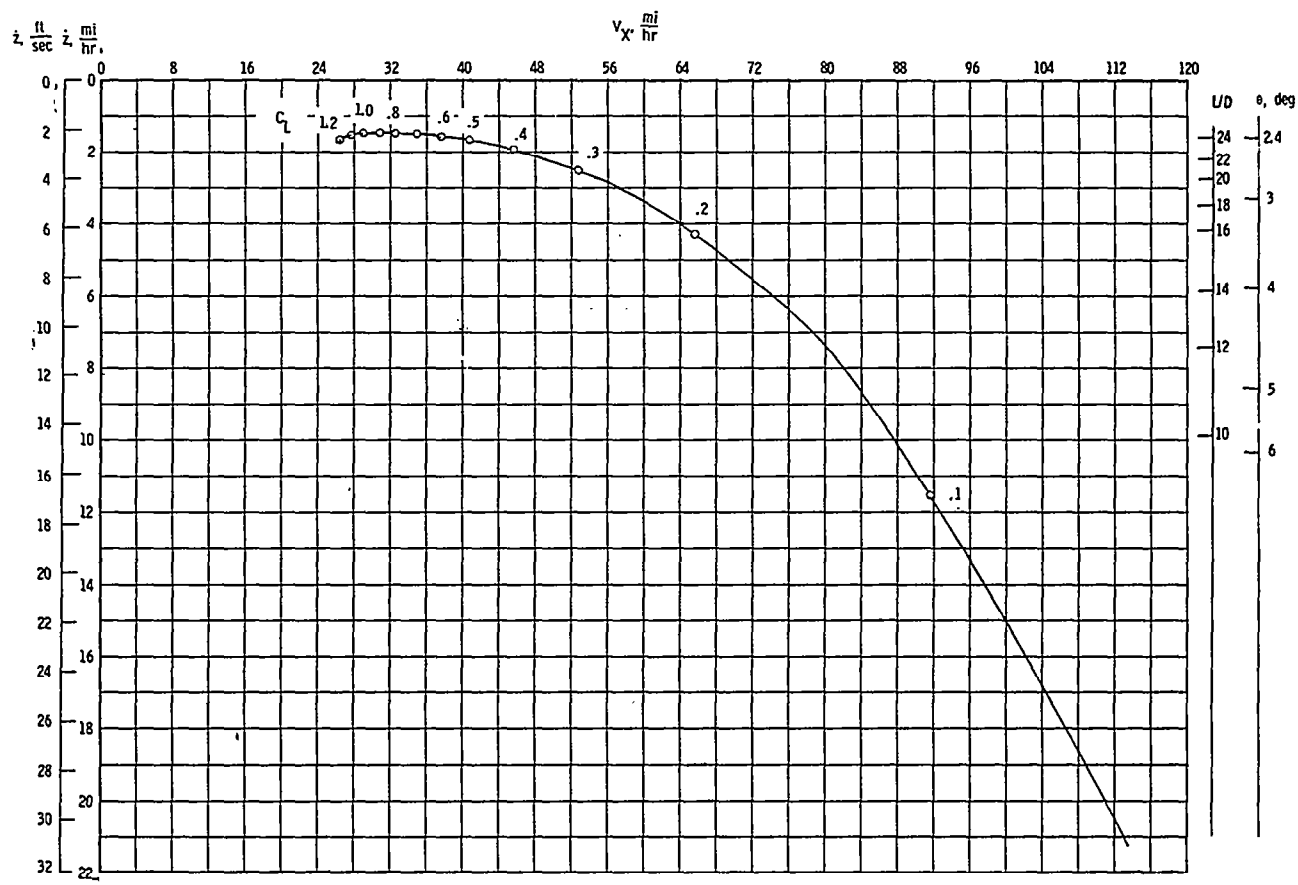

Figure 14.- Gliding diagram for design with b = 40 feet and A = 8.

addition of ballast the value of φ^* or $C_L{}^*$ that corresponded to a given value of r will now have that same value for r_b, where r_b is given by equation (33).

ADVANCED APPROACHES TO DESIGN PROBLEMS

The foregoing analysis has given a picture of the various problems and conflicts involved in designing a sailplane for high efficiency in circling flight while maintaining reasonably efficient gliding capabilities and has indicated the extent to which these problems may be solved by using current sailplane technology. Although it appears that an efficient soaring plane can be built by using conventional methods, this craft still does not approach the overall efficiencies ultimately desired. The possibilities for future improvements therefore must be considered. Since the basic concern is with the design of the thermal soaring plane, the possible improvements of circling flight are discussed primarily, but means for increasing gliding efficiency are also considered.

The improvement of circling efficiency can be attained by decreasing the magnitude of the sinking velocity as a function of r. The relations involved are given by the performance equations (5) and (6). Each of the structural and aerodynamic factors therein will be examined to see where improvement possibilities exist.

Reduction of Wing Loading

The first obvious improvement needed for increased circling performance is a reduction of the wing loading without making such structural changes as will cause an increase in drag. This reduction can, of course, be accomplished by a reduction in the magnitudes of the basic weight W_o and the structural weight coefficients γ_S, γ_b, and γ_f. Since W_o is fixed for a given pilot and his equipment, little can be done except to make use of miniaturized equipment and lightweight parachute packs. The wing-area weight coefficient γ_S can probably be reduced by applying the new technique of using an extremely thin wing skin supported internally by a light foamed plastic. This technique, when fully developed, can result in a wing of high structural efficiency as well as aiding in the maintenance of perfect profile contours under load.

The spar weight coefficient γ_b can be reduced by development and utilization of new structural materials with a very small value of the elasticity-weight parameter $\frac{\rho_w}{E^{1/2}}$, where ρ_w is the weight density. At present, aluminum alloys offer the lowest values, but with the great strides being made in solid-state physics and polymer chemistry, considerable improvements in structural metals and plastics may not be too far away. In reality, complete elimination of the wing spar and ribs may not be beyond the realm of foreseeable application with

the new fiber-glass and resin fabrication techniques already in use for the manufacture of certain aircraft parts. (See refs. 7 and 8.)

Of course, certain special wings have long been made without ribs or spars by use of air-inflated wing shells. The difficulty of obtaining and maintaining an efficient profile and the drag caused by the external bracing usually required with these wings have precluded their use on sailplanes. Further development in the weaving of such shells by use of additional and more accurate drop cords, combined with internal bracing, can possibly make an efficient wing for sailplane use, especially for the small-span soaring plane. Reductions in γ_s and γ_b are very important since together they presently contribute up to 50 percent of the total wing loading of many sailplanes.

The source of the coefficient γ_f is particularly amenable to reduction and offers the simultaneous advantage of lower drag. Since γ_f is associated with the fuselage and empennage structure, both of which contribute heavily to the parasite drag, any reduction or elimination of these components will be doubly beneficial. An optimum design would, of course, be the flying wing, as has long been appreciated, but various practical requirements usually demand some amount of fuselage and empennage structure. The primary need for the long fuselages used on present sailplanes, outside of the small section needed to house the pilot, is to support the vertical tail at such a distance from the center of gravity as to give directional stability and sufficient rudder control to overcome the severe adverse yaw which usually occurs with large-span high-aspect-ratio wings. Even with the long tail lengths used, a large vertical-tail area is still required for directional stability. The fuselage also supports the horizontal tail but a long horizontal tail length is not actually essential if proper location of the center of gravity is made. With the small-span thermal soaring plane it should be possible to reduce considerably or even eliminate the need for the vertical tail and aft fuselage and thus obtain appreciable gains in circling performance and maneuverability. As has already been discussed, a large vertical tail is undesirable in small turns for stability reasons. In this connection it should be noted that birds do not use vertical tails and that the body length of all efficient soaring birds is especially short; therefore, the wings play the dominant role in effecting stability and control. It appears that numerous possibilities exist for lowering the minimum wing loading of the thermal soaring plane, and that many of these also have favorable drag reduction effects.

Although it may appear that it is somewhat unnecessary to strive for any great reductions in wing loading, because of the requirements for gliding penetration, this is not the case since the wing loading of a craft can be increased to meet specific wind conditions by addition of ballast, and a low minimum wing loading will leave the craft free for attaining the maximum soaring efficiency on calm days. In addition, the possible use of variable geometry, to be discussed subsequently, requires a very minimum structural weight for all components in order that a low basic wing loading would be attainable. In general, gross wing loads as low as 1.00 pound per square foot would be very desirable.

Improvement of Aspect Ratio

The next parameter for consideration is the aspect ratio A, which is of primary importance since it critically affects both wing loading and drag. To obtain a low value for $\dot{z}$, it is necessary to have a large A, but a large A means a high value for W/S with a fixed span length. Thus, as has been previously discussed, some compromise of circling efficiency is inevitable. There appears, however, a possible way of alleviating this restriction somewhat by using the method employed by the land soaring birds such as the hawk and the vulture. The method used by the bird is the slotted wing tip, a feature characteristic of all the larger land soarers. Although the aerodynamics of this mechanism are very involved and include complex aeroelastic effects, it appears worthy of investigation as a means for advancing sailplane performance.

The problem which the bird wing appears to solve is that of obtaining a high effective aspect ratio kA with a wing of low geometrical aspect ratio. This condition, of course, requires that k be greater than 1.0. The outer third of each semispan of the wing is composed of seven to nine separate pinions, each acting as an individual airfoil. The first three or four leading pinions have a very elastic rachis, or spar, and a large amount of wash-in near the tips so that under the airload of flight, they have a pronounced span curvature. (See fig. 15.) Such an arrangement allows a separate vortex sheet to emanate from each pinion with a consequent spreading of the trailing vorticity over a large vertical area. (See fig. 16.) The resulting lowering of the effective "downwash" velocity at each point of the total wing system considerably reduces the overall induced drag.

(a) Wing.

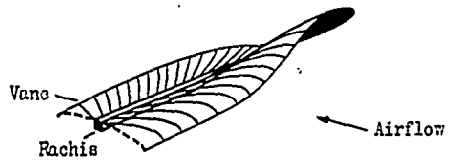

(b) Detail of pinion tip wash-in.

Figure 15.- Wing of a land soaring bird.

The problem of determining the maximum effective aspect ratio, or efficiency factor k, of such a branched-tip wing system can be solved by use of the electrical potential flow analog for the simulation of the vortex wake. This has been done for a form representing a typical branched-tip configuration. (See fig. 17.) The value of k for this system is 1.35, which means that this wing, when optimally loaded, will have 25 percent less induced drag than even the most efficient flat elliptical wing having equal projected span and lift. Since the induced drag makes up a very large percentage of the total drag in small turns, this drag reduction can be important in reducing the sinking velocity in small turns. The value of such a mechanism in increasing the aerodynamic efficiency of a wing of limited span is obvious. A discussion of the theoretical and design aspects of nonplanar wing systems of the type discussed appears in references 9, 10, and 11.

Reduction of $C_{D,\infty}$ and $C_{D,p}$

Since $C_{D,\infty}$ reflects primarily the skin friction and pressure drag of the wing, most improvements here must come primarily from the development and perfection of construction techniques for laminar-flow profiles, especially those possessing an extensive drag bucket which extends to very high lift coefficients. As has been discussed previously, several valuable profiles already exist for this application, but more work is needed, particularly for the high lift design range. Another source of improvement lies in the perfection of more efficient control systems, both aileron and elevator controls. The use of the flap-type aileron control is especially inefficient even when the control gap is sealed, since strong vortices are still shed from the lateral edges of both the aileron and wing and cause reduced aileron efficiency and loss of wing lift. Development of lateral control by wing-tip warping or by use of variable camber in the wing-tip sections would be a great improvement since full continuity of the surface would be preserved. Complete elimination of conventional rudder and elevator controls would be even more desirable from the drag, weight, and stability viewpoint of circling flight.

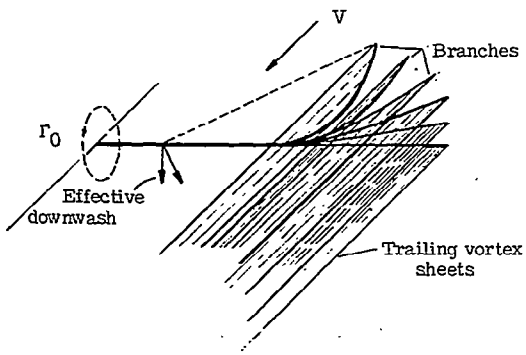

Figure 16.- Vortex sheet pattern for branched tip.

Reductions in the parasite drag coefficient $C_{D,p}$ can come from careful attention to such important matters as wing-fuselage juncture design to prevent separation and preserve the wing lift distribution, canopy design for streamline flow, and elimination of all surface gaps and protuberances. Elimination of as much fuselage (an empennage) area as is practical would be advantageous, provided the resulting fuselage fineness ratio is not small enough to cause afterbody separation with a large pressure drag. The maintenance of as much laminar flow as possible without premature separation at high lifts must be the design aim.

Improvement of Gliding Efficiency

The various means which have been discussed for improving circling efficiency will, in general, also be beneficial in increasing gliding performance. However, the primary gliding requirements, a high lift-drag ratio and moderately high ground speed, necessitate the use of high aspect ratio and wing loading, which is directly opposed to the low wing loading required for thermal soaring. The only obvious possibility for achieving maximum performance in both areas lies in the application of variable geometry to give the optimum wing loading for each phase. The ideal solution to this problem obviously lies in a

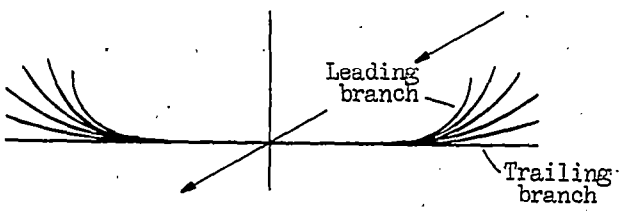

Figure 17.- Analog representation of branched-tip vortex system.

variable-area, variable-aspect-ratio wing which could be used in the large S, small A condition for circling and in the small S, large A condition for gliding. This could be most easily accomplished by use of a large, full-span Fowler type flap. The basic wing could be designed for optimum soaring performance with the lowest possible wing loading. Then a large percentage, as much as 30 to 40 percent, of the trailing part of the wing could be designed to retract into the main wing to reduce the wing area and simultaneously increase the aspect ratio for efficient gliding. The design and construction of such a wing would no doubt be very complex, especially since the parasite drag must be kept to an absolute minimum. The added structural weight that would most probably occur with such a variable-geometry airfoil makes the foregoing weight-reduction possibilities all the more important in order that a very low overall wing loading will be attained.

Other methods for accomplishing these requirements are possible. For example, the soaring bird reduces his wing area for a fast glide by partially flexing his wings so that much of the basic area of the secondary feathers overlaps. The resulting cranked wing not only reduces the wing area but also appears to serve the trim and stability needs for the high-speed flight.

CONCLUDING REMARKS

It has been the intention of this paper to discuss the concept and potentialities of the thermal sailplane as a means for increasing the reliability and certainty of local soaring flight and to outline in a general way a procedure by which the optimum design of such a craft can be determined. An attempt has been made to relate in a quantitative manner the relevant meteorological, structural, and aerodynamic factors involved in thermal soaring flight so as to best satisfy nature's requirements for efficient use of the thermal energy in vortex shell convections. The problems and conflicts arising in the design of a sailplane for high performance in both the soaring and gliding phases of flight have also been considered, and various compromises and ideal solutions discussed.

The considerations in this paper indicate that despite the handicap of insufficient quantitative thermal data for design purposes, enough information can be obtained from various sources to proceed with the design and construction of a conventional-geometry thermal sailplane capable of very high performance in soaring flight and with satisfactory gliding and penetration abilities. Such a plane can serve as a research vehicle for gathering the thermal data needed for more optimum designs. With such a tool as the thermal sailplane, much generally valuable information on the meteorological structure and properties of the lower atmosphere can be obtained.

Langley Research Center,
National Aeronautics and Space Administration,
Langley Station, Hampton, Va., September 19, 1963.

APPENDIX A

STABILITY OF CIRCLING FLIGHT

Unlike the relatively simple aerodynamics of a spiral glide in still air, circling flight within thermals is very complex and this complexity is compounded when the size of the thermal shell approaches the same order of magnitude as the wing span of the sailplane.

Effects Encountered in Large Thermals

First consider the effects of circling in the interior of a thermal which is very large compared with the span, that is, $R/b \gg 1$. (See fig. 18.) In this case, the craft will be circling in an essentially uniform upcurrent. As the craft circles, the outer wing tip travels faster relative to the air than does the inner tip, with a resultant difference in dynamic pressure which is proportional to the difference in the squares of the tip velocities. A simple analysis shows that the ratio of the dynamic pressure q_o at the outer wing tip to that at the inner wing tip q_i is given approximately by

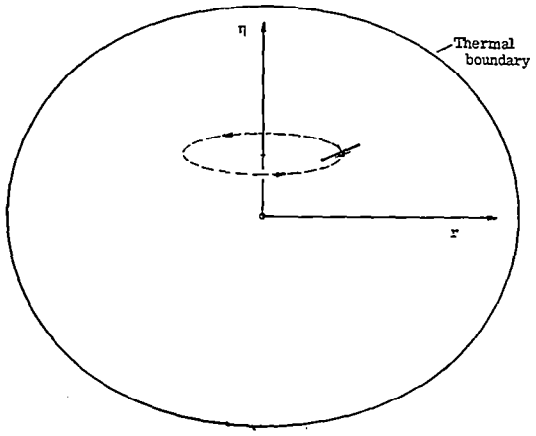

Figure 18.- Sailplane circling in a large thermal.

$$\frac{q_o}{q_i} = \frac{\left(1 + \frac{b}{2r}\cos\varphi\right)^2}{\left(1 - \frac{b}{2r}\cos\varphi\right)^2} \qquad \text{(A1)}$$

where φ is the bank angle and r is the radius of turn. This relation is plotted in figure 19 for a range of values of φ. It is obvious that this ratio can attain very large values for large values of the relative-size factor $\frac{b}{2r}\cos\varphi$, corresponding to small turns with a small bank angle ($\cos\varphi \to 1$). This large q-difference can produce a very strong rolling moment into the turn.

Without any compensating effects, a sailplane in a really tight turn (r/b approaching $1/2$) would continue to bank until a stall and spin developed, despite aileron control. Two secondary factors, however, help reduce this unstable moment. First, since the inner wing is traveling at a lower circling velocity, it will experience a higher angle of attack than the outer wing, as shown in figure 20. This condition will help to counteract the q-difference effect. Quantitatively, the angle-of-attack variation $\alpha(y)$ across the span in a turn is given by

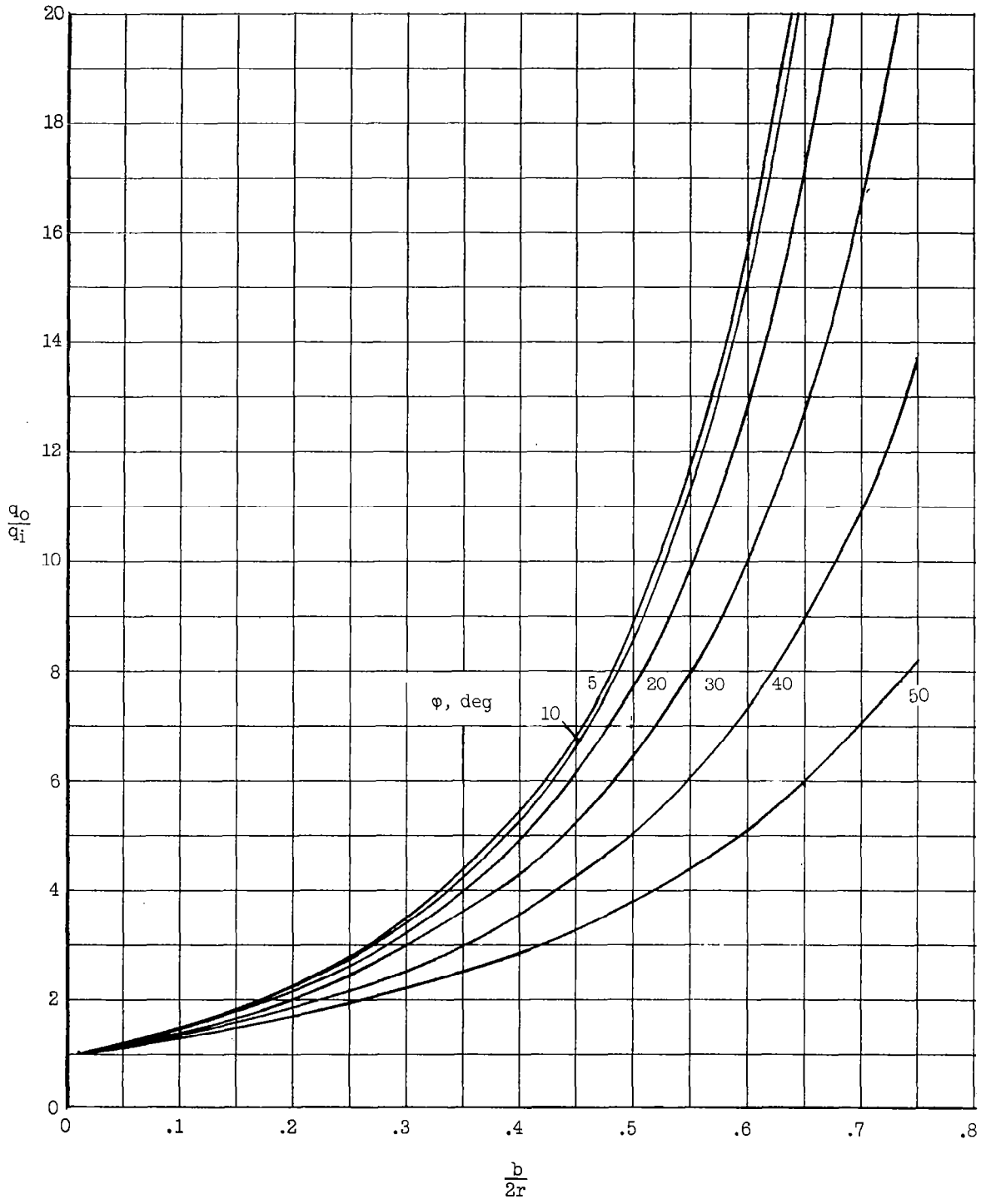

Figure 19.- Variation of dynamic pressure ratio with radius of turn parameter.

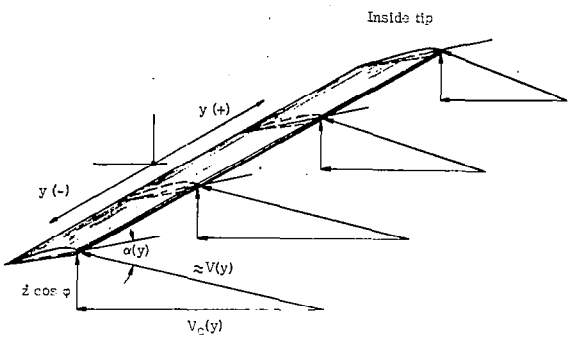

Figure 20.- Representation of resultant velocity and angle-of-attack variation across span of a circling wing.

$$\alpha(y) = \alpha_o + \frac{\dot{z} \cos \varphi}{V_c\left(1 - \frac{y}{r} \cos \varphi\right)} \qquad (A2)$$

where α_o is the effective angle of attack at the center of the wing, V_c is the circling velocity of the sailplane, and y is the distance measured from the plane of symmetry and is positive in the direction of the inside wing tip.

The result of the combined dynamic pressure and angle-of-attack effects is that a net unstable rolling moment still exists. The two effects combine to produce a spanwise lift loading which can be expressed as follows:

$$L'(y) = \pi\rho c\alpha_o V_c^2\left(1 - \frac{y}{r} \cos \varphi\right)^2 + \pi\rho c V_c \dot{z} \cos \varphi\left(1 - \frac{y}{r} \cos \varphi\right) \qquad (A3)$$

and it is evident from inspection of the second term on the right that the effects of the dynamic pressure decrease on the inside wing and overcome those of the angle-of-attack increase. Thus, a net rolling moment l into the turn will still exist in the magnitude of

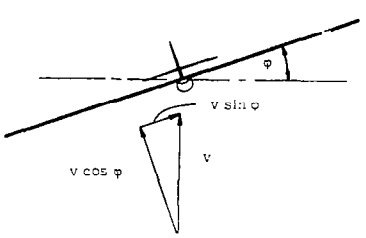

(a) Sideslip velocity.

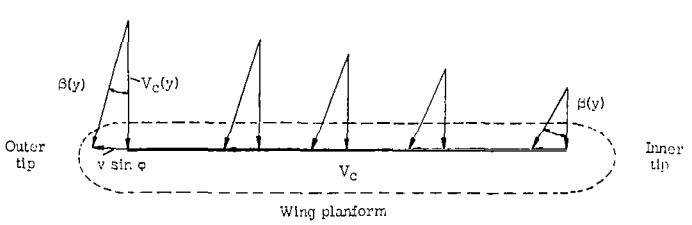

(b) Sideslip angle.

Figure 21.- Sideslip velocity V sin φ due to angle of bank.

$$l = \int_{-b/2}^{b/2} L'(y)\, y\, dy \qquad (A4)$$

Equations (A3) and (A4) may be used to calculate the approximate value of this unstable moment for a given wing in circling flight.

A second effect exists, however, which usually makes circling flight stable. Because of the large bank angles necessary for such small turns that q-effects are significant, the upcurrent actually produces a component of sideslip velocity V sin φ as shown in figure 21(a). The angle of sideslip β thus produced varies across the span because of the difference in tip speeds. (See fig. 21(b).) This sideslip velocity acts on both

the wing and vertical tail to produce rolling moments opposing the bank. The vertical tail can contribute a strong negative input to the effective dihedral $\partial C_l/\partial\beta$, and the decreasing effective angle of sideslip on the outer wing causes a piling up of the boundary layer near the tip stations and may ultimately cause the tip region to stall in tight turns, provided the span is large enough. The crossflow can also lead to flow separation on the fuselage nose and canopy with detrimental effects of the wake on the lift of the outer wing. A yawing moment into the turn will also be produced by the tail side force but this effect is somewhat balanced by the side force on the nose and asymmetric wing drag. Thus, for sailplanes with high wing loadings and large spans, with resulting large values for the minimum radius of turn (such as characterized by modern designs), these secondary stabilizing effects tend to delay the ultimate onset of the unstable rolling moment in small turns. The very high wing loadings of current large-span sailplanes limit the minimum radius of turn to such large values that roll instability effects are scarcely noticeable, and only moderate, if any, aileron control is necessary to hold "tight" turns.

For large-span sailplanes with low wing loadings, however, the stability picture is very different. With such loadings the q-effects become very significant because of the relatively small minimum radius of turn which can be made and the favorable sideslip effects diminish because the craft does not have to bank as much to attain a given radius of turn as with a heavier loading. The angle-of-attack effects also increase but may now become detrimental. Because of the low speed of the inner wing, the airfoil section Reynolds number is lowered, with an accompanying decrease in the maximum section lift coefficient. Ultimately, a point is reached where the inner tip stalls and the craft goes into a spin. Several of the early German sailplanes having very low wing loadings and very large spans were actually victims of this phenomenon. It should be noted that such adverse effects depend upon the combination of both large span and low wing loading. Combinations of large span and high wing loading or small span and low wing loading can alleviate these dangers considerably. These facts must be carefully considered in designing a thermal sailplane.

Effects Encountered in Small Thermals

Consider now the situation which will be encountered by a sailplane circling in a thermal whose size is of the same order as the wing span, that is, a large-span sailplane in a small thermal, as shown in figure 22. This condition, of course, presupposes the craft to have a sufficiently low wing loading. The craft will no longer be circling in a uniform upcurrent, and the effective aerodynamic velocity will vary all across the span because of the variations in the air current. The same effects as previously discussed will still exist, but because the span extends over a large percentage of the thermal, the velocity of the upflow will decrease across the span and tend to load the inner wing and unload the outer

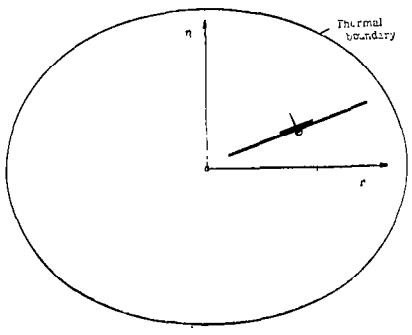

Figure 22.- Sailplane circling in a small thermal.

wing. Depending upon the relative sizes of the thermal and span, this stable loading trend can become very detrimental to efficient soaring. If the span is too large, such a strong stable rolling moment will be produced that the craft cannot possibly hold the bank necessary to circle within the shell. In fact, if the desired bank is obtained by some means such as use of initial rolling momentum, the inner wing will be promptly lifted and the plane rolled back out of the turn. On the other hand, the danger of stalling the inner wing exists. Thus, there are two extremes, too much stability and complete instability, operating very close to one another. In this case, the effects of the radial flow components, as shown in figure 23, must also be considered. This flow produces not only a sideslip velocity but also a component normal to the span which, in the top half of the thermal, acts to decrease the angle of attack. For large spans, the outer wing will be primarily affected by this radial flow, and, as a result, there is a decrease in its loading and a rolling moment opposing the turn. The combined effects of the vertical and radial components on large spans in small thermals can thus produce such high stability that it may be impossible to circle within the thermal, even with full use of ailerons, and the thermal energy cannot be used.

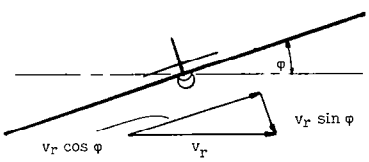

Figure 23.- Velocity components due to the radial flow v_r.

Estimation of Stability Effects

These stability effects can be estimated in a quantitative manner, provided the necessary thermal data are available. For example, if the bank angle φ and coordinates r_c, η_c of the flight path of a given sailplane in a given thermal are established or assumed, then to each point of the span there may be assigned a position r, η as shown in figure 24(a). Analytically, the line segment representing the span can be simply expressed as

$$\eta_b = r_b \tan \varphi + \eta_o \tag{A5}$$

between the limits

$$r_c - \frac{b}{2} \cos \varphi \leqq r_b \leqq r_c + \frac{b}{2} \cos \varphi \tag{A6}$$

where η_b, r_b are variable-span coordinates referred to the thermal origin, η_o is the η-intercept of the span extended, and r_c is the radius of turn. The entire span can then be transformed to an equivalent curve on the thermal diagram by placing the various r_b, η_b points at the corresponding r, η positions on the dimensional thermal diagram, and the variation of vertical (or radial) velocity across the span read directly, as shown in figure 24(b). With these values, the lift loading and rolling moment can be estimated.

In addition to stability effects occurring with large spans, there exist the accompanying increases in trim, separation, and induced drags. These increases can so increase the sinking velocity that the very reason for having a large span is no longer valid, insofar as circling flight is concerned.

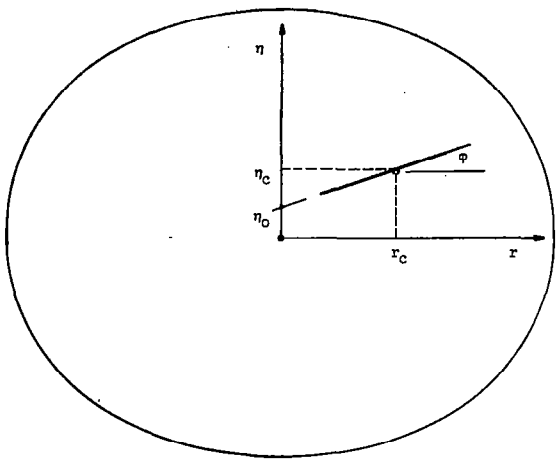

(a) Space diagram.

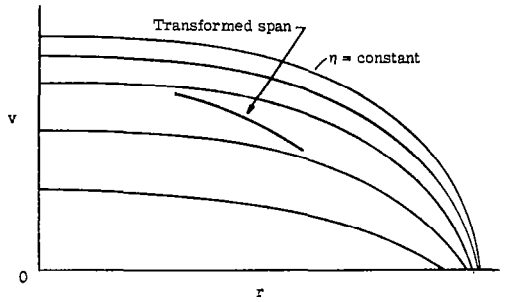

(b) Velocity diagram with transformed span.

Figure 24.- Diagrams for determining velocity distribution across span in small thermals.

It is clear from the foregoing considerations that large-span sailplanes attempting to operate in small thermals may expect to encounter many adverse effects. The exact nature and magnitude of these effects will depend upon the relative size of the thermal and span and upon the thermal strength, and even with a full knowledge of thermal characteristics, the complete aerodynamic analysis of such a flight will still be very lengthy and complex. In fact, much of the necessary aerodynamic theory, such as the induced-velocity field of the spiral asymmetric vortex sheet produced by a circling sailplane in small turns, has not even been developed; thus, only crude approximations of many of the effects can be made.

The obvious and necessary conclusion is that the thermal soaring plane must be designed with a span that is small compared with the minimum thermal size in which it is intended to operate with full efficiency.

APPENDIX B

THERMAL DISTRIBUTIONS

If large and powerful thermals were very numerous at all places and at all times of the day and year, existing sailplane designs would be quite sufficient and there would be no need for a special sailplane to increase the certainty of flight. Obviously, such is not the case. The facts point to the conclusion that, on a relative-size basis, small thermals make up the larger percentage of the total thermal production. This is also obvious from elementary considerations. Surface heating produces only a limited volume of buoyant air in a given time interval so that the size of the thermals produced from this air will depend upon the number of total thermals formed. If the thermals are large, only a few can be formed; thus, the frequency of production will be low. If they are small, the frequency of formation will be high. The production of large thermals requires that the heated air layer (ref. 2) be held in an unstable equilibrium for a relatively long time while sufficient warm air accumulates. The maintenance of such an equilibrium for any appreciable length of time is generally impossible because of the continuous generation of turbulence in the lower air layers by the horizontal air motion. This action strongly favors the production of many small thermals. The large thermals which occur over the southwestern part of this country in late summer and in tropical desert regions are due to the very high rates of surface heating in those regions, where large volumes of hot air are produced very rapidly. Unfortunately for soaring, such areas in this country are very limited since vegetative cover reduces surface temperatures appreciably.

Thermal Frequency Diagram

In general, one would expect for a given type of surface terrain and surface heating rate one thermal size or range of sizes to be produced with a higher frequency (number of thermals per unit surface area per unit time) than other sizes, the frequency tending to zero for larger or smaller thermals on either side of this maximum-frequency size. The generalized form of such a distribution is shown in figure 25(a), where the thermal size of maximum frequency has been identified as R', and σ is the formation frequency. The value of R' is most probably a strong function of the type of terrain and strength of the prevailing wind. In addition, the values of both σ' and R' are no doubt very strong functions of the time of the day and year because of the variation of the surface heating rate. The whole secret of attaining a high degree of certainty in soaring flight lies in the ability of sailplanes to accomplish equilibrium flight in a small enough thermal that the production frequency and distribution of this size and all larger thermals is sufficient to guarantee a high probability that a usable thermal can be intercepted in sufficient time when needed for altitude gain.

The determination of a minimum-size thermal to use as a design basis for a thermal soaring craft depends very much upon the magnitude of σ for each thermal size. For example, if σ were sufficiently large for even very large

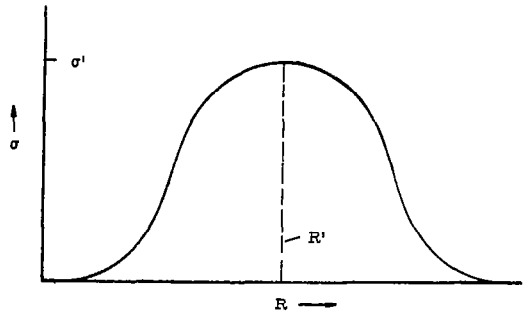

(a) Thermal size of maximum frequency.

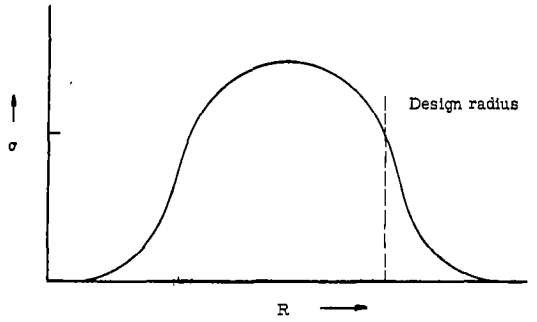

(b) "Design" thermal size.

Figure 25.- Thermal production frequency diagram.

thermals, there would be no need to design for use of the smaller thermals even though they make up by far the greater percentage of the total thermal production. This condition is illustrated in figure 25(b) where the "design" thermal size occurs near the upper size limit. Unfortunately, modern sailplanes have made it clear that, except for a few exceptional areas during the hottest summer months, the production frequency of sufficiently large thermals is far below their soaring needs.

Fundamental Hypothesis of Soaring Reliability

It therefore appears that the solution to increased soaring certainty and efficiency lies in the development of a sailplane capable of performing turns of very small radius while still maintaining a relatively low sinking velocity. Then a very large range of thermal sizes and strengths[2] will become available for use, and the certainty of flight will greatly increase. Indeed, it is true that the only reason an improvement in the certainty of soaring flight can be expected is that the atmosphere is filled during the day with a large number of small thermals rather than a few large ones. This statement might be rephrased as the "fundamental reliability hypothesis" of thermal soaring: The production frequency and spatial distribution of small thermals in the atmosphere is sufficiently great that an aircraft which can attain equilibrium in small thermals will be capable of increased certainty of sustained flight compared with a craft which can use only the larger thermals. The validity of this hypothesis is well supported by existing data.

[2]No mention has been made here of the range of thermal-strength variation which may occur for a given thermal size; this variation is an important but secondary problem. The thermal sailplane must always be designed for use of very weak thermals.

REFERENCES

1. Cone, Clarence D., Jr.: Thermal Soaring of Birds. American Scientist, vol. 50, no. 1, Mar. 1962, pp. 180-209.

2. Cone, Clarence D., Jr.: The Theory of Soaring Flight in Vortex Shells. Soaring, vol. 25,
   Pt. I, no. 4, Apr. 1961, pp. 8-13.
   Pt. II, no. 5, May 1961, pp. 8-12.
   Pt. III, no. 6, June 1961, pp. 6-8.

3. Cone, Clarence D., Jr.: A Theoretical Investigation of Vortex-Sheet Deformation Behind a Highly Loaded Wing and Its Effect on Lift. NASA TN D-657, 1961.

4. Wilkinson, K. G.: The Design of Sailplanes for High Performance. Aircraft Eng., vol. XXIII, no. 271, Sept. 1951, pp. 263-271.

5. Abbott, Ira H., and Von Doenhoff, Albert E.: Theory of Wing Sections. Dover Pub., Inc., 1959.

6. Abbott, Ira H., Von Doenhoff, Albert E., and Stivers, Louis S., Jr.: Summary of Airfoil Data. NACA Rep. 824, 1945. (Supersedes NACA WR L-560.)

7. Anon.: Glass Fiber V/STOL Propeller Is Tested. Aviation Week, vol. 74, no. 25, June 19, 1961, pp. 93, 95.

8. Anderton, David A.: Glass-Fiber Blade Boosts Endurance 70%. Aviation Week, vol. 74, no. 15, Apr. 10, 1961, pp. 67, 69.

9. Cone, Clarence D., Jr.: The Theory of Induced Lift and Minimum Induced Drag of Nonplanar Lifting Systems. NASA TR R-139, 1962.

10. Cone, Clarence D., Jr.: The Aerodynamic Design of Wings With Cambered Span Having Minimum Induced Drag. NASA TR R-152, 1963.

11. Cone, Clarence D., Jr.: The Bending-Moment Distribution of Cambered-Span Wing Systems Having Minimum Induced Drag. NASA TN D-1505, 1963.

NASA-Langley, 1964 L-3306